current issues in molecular biology

MDPI

Article

Mathematical Modeling of Sperm Survival: Analysis of Interactions Between Thermal Stress, Oxidative Doses, and ROS Kinetics

Manal Abouelouafa [1], Anas Mbarki [2,*], Soufian Omari [2], Aziz Ettahir [2], Brahim El Houate [3], Youssef Bakri [1] and Hicham El Ossmani [1]

[1] Laboratory of Human Pathology Biology, Faculty of Sciences, Mohammed V University, Rabat 10100, Morocco; abouelouafa.manal@gmail.com (M.A.); y.bakri@um5r.ac.ma (Y.B.); helossmani@yahoo.fr (H.E.O.)
[2] Materials, Energy and Acoustics Team (MEAT), École Supérieure de Technologie de Salé, Mohammed V University in Rabat, Salé 11060, Morocco; soufianmouhamed15@gmail.com (S.O.)
[3] Biological and Health Sciences Team, Higher Institute of Nursing Professions and Health Techniques, Ouarzazate 45000, Morocco; belhouate@gmail.com
* Correspondence: anas.mbarki.y@gmail.com

Abstract

Background: Reactive oxygen species (ROS) are required for normal sperm function, but when they accumulate, they cause oxidative stress, DNA damage, impaired motility, and loss of viability. Heat stress—scrotal hyperthermia, in particular—also degrades sperm quality. How thermal and oxidative stress jointly lead to sperm dysfunction is still poorly understood, which hinders the setting of evidence-based occupational exposure limits and the design of sperm preservation protocols. **Objective:** We developed a mathematical framework that combines oxidative stress (ROS kinetics) with thermal stress (heat diffusion) to estimate sperm survival and to derive dose–response relationships. The model is meant to generate hypotheses that independent experiments can test; it is not a validated clinical predictor of male infertility. **Materials and methods:** Exposure ranges, biological thresholds, and dose–response parameters were taken from published in vitro studies on human and animal sperm (1995–2024). Records were retrieved from PubMed and Web of Science with the search terms "ROS sperm", "thermal stress male reproduction", and "hydrogen peroxide spermatozoa". Studies were retained if they quantified ROS concentration, H_2O_2 exposure, or thermal dose in relation to sperm motility, viability, or DNA integrity; reviews, single case reports, and studies without quantitative dose–response data were excluded. Each data set was labeled by species (human, rat, bull, and others) and by sperm source (ejaculated or testicular), and differences in experimental conditions, medium composition, and temperature were recorded. A probit model was combined with a diffusion–reaction equation for ROS and with Fourier's heat equation to simulate predefined exposure scenarios. The Python 3.14.5 script was compiled in the online interface, was used for probit fitting and plotting. To reflect differences in cellular antioxidant capacity, protected, normal, and vulnerable sperm were modeled as three separate phenotypic populations. **Results:** Predicted survival depended mainly on ROS concentration, thermal dose, and exposure time. Changing the rates of ROS generation and degradation altered the predicted oxidative exposure and survival probability appreciably. In the thermal simulations, viability declined with increasing dose, and the critical thermal distance varied inversely with thermal severity. The model separated four biological zones: signaling (about 100 nM H_2O_2), impaired motility (15 μM H_2O_2, roughly 1–2 h of exposure), DNA damage (50 μM H_2O_2), and lethality (≥200 μM H_2O_2). Antioxidant capacity and exposure duration strongly shaped the response to both oxidative and thermal stress. **Conclusions:** Sperm

Check for updates

Academic Editor: Violeta Popovici

Received: 23 July 2026
Revised: 19 October 2026
Accepted: 21 October 2026
Published: 4 November 2026

Copyright: © 2026 by the authors. Licensee MDPI, Basel, Switzerland. This article is an open access article distributed under the terms and conditions of the Creative Commons Attribution (CC BY) license.

survival depends strongly on the magnitude and duration of oxidative and thermal exposure. The framework offers a quantitative basis for studying stress-dependent changes in sperm viability and yields hypotheses that can be tested experimentally. Before any clinical use, it needs independent validation under standardized, prospectively defined protocols; for now, it serves as a research tool for generating hypotheses and comparing exposures.

Keywords: reactive oxygen species (ROS); oxidative stress dose; lethal thermal dose; morph-functional spermatozoa; male infertility; sperm survival probability

1. Introduction

1.1. Overview of Male Infertility

Male infertility affects approximately 15–20% of couples globally, with reduced sperm quality contributing to half of these cases. Among the modifiable risk factors, elevated scrotal temperature represents one of the most preventable causes of spermatogenic dysfunction. Contemporary occupational environments (prolonged computing, welding, and vehicles in high-temperature regions) expose workers to sustained heat stress that can reduce sperm production. Understanding the mechanistic pathways linking thermal stress to sperm dysfunction—particularly through oxidative stress—is therefore crucial for both clinical interventions and occupational health policy.

1.2. Thermal and Oxidative Stress: Causes and Mechanistic Pathways

Temperature and male fertility: Work on this subject includes studies of repeated rises in core body temperature and human sperm production [1], of the effects of hyperthermia and hypothermia on spontaneous contractions of the testicular capsule [2], and of the association between higher temperature and suppressed spermatogenesis [3]. Prolonged testicular hyperthermia can halt spermatogenesis altogether [4]. Epidemiological and clinical studies repeatedly report temporary infertility in men exposed to sustained heat, an effect said to be stronger in men [5,6]. Sperm density, motility, and the proportion of normally shaped cells all decline when scrotal temperature rises above the physiological range [2,7–11].

Oxidative stress and ROS-mediated damage: Excess ROS can cause double-strand breaks in nuclear and mitochondrial DNA, alter the citrullination state of protamine's, and may contribute to Y chromosome microdeletions (Y-MD), notably in the AZF (azoospermia factor) regions needed for spermatogenesis [11–13]. Human spermatozoa are especially exposed because their cytoplasm holds little antioxidant enzyme activity. At physiological levels, however, ROS such as hydrogen peroxide (H_2O_2) act as signals in capacitation and in the acrosome reaction [14]. Beyond that range, they irreversibly damage the lipid bilayer of the sperm membrane, denature flagellar proteins, and fragment nuclear DNA.

Thermal–oxidative coupling: Heat acts as an environmental trigger that drives oxidative stress, and oxidative stress, in turn, becomes the main chemical mediator of cellular injury. Three mechanisms explain how heat raises ROS levels. First, it disturbs the mitochondrial electron transport chain in germ cells and Sertoli cells, so that electrons leak and superoxide anion forms in large amounts. Second, it upregulates enzymes, adding to free radical production. Third, it lowers the expression of antioxidant enzymes (catalase, superoxide dismutase, and glutathione peroxidase) and leaves cells poorly protected. The ROS produced in this way attack polyunsaturated fatty acids in sperm and germ cell membranes, thus reducing membrane fluidity and weakening Sertoli cell tight junctions; the blood–testis barrier and the immunological protection of developing germ cells are

compromised as a result. When heat and ROS act together, they can exceed the capacity of heat shock proteins, so denatured proteins are not repaired and mitochondria-dependent apoptosis is triggered.

Variability of ROS dose–response relationships: Reported ROS sensitivity of spermatozoa varies a great deal. High concentrations affect motility, ATP production, lipid peroxidation, and DNA fragmentation, but the size of the effect depends on exposure time, medium composition, the endpoint measured, antioxidant conditions, and whether exposure occurs in vitro or in vivo [11,15]. The literature describes graded, concentration-dependent responses and does not support a single universal toxicity threshold. For instance, H_2O_2 in the sub-micromolar range has been linked to changes in motility and DNA integrity under particular experimental conditions [15–17]. Such values are best read as thresholds tied to specific conditions, not as general limits for human sperm survival or male fertility. Thresholds that come out of modeling studies are likewise specific to species and conditions, and they need confirmation with human data.

1.3. Experimental Models from the Literature

Experimental data published between 1995 and 2024 were retrieved from PubMed, Web of Science, and Google Scholar with the terms "ROS sperm", "hydrogen peroxide spermatozoa", "thermal stress male fertility", and "occupational hyperthermia reproduction". Peer-reviewed studies were included if they quantified ROS concentration (usually as H_2O_2 in μM); exposure duration; and sperm endpoints, such as motility, viability, DNA fragmentation, or mitochondrial potential. Reviews, editorials, case reports, and studies without quantitative dose–response data were excluded. Human data (ejaculated sperm and testicular biopsy specimens) and animal data (rat, bull, and mouse) were compiled together but labeled by species and tissue source.

Human data: In vitro studies of human ejaculated sperm exposed to defined H_2O_2 concentrations under standardized conditions (physiological pH, isotonic medium, and 37 °C) show effects that become more severe as the dose rises. At about 100 nM H_2O_2, ROS behave as second messengers, which defines the signaling threshold. Motility is impaired at 15 μM after roughly 1–2 h, DNA damage appears at 50 μM, and concentrations of 200 μM or more are lethal, with DNA fragmentation and mitochondrial dysfunction.

Animal data: Studies in rats, bulls, and mice have clarified the mechanisms of thermal injury and ROS kinetics, but these species differ from humans in testicular anatomy, thermoregulation, and sperm characteristics. Extrapolation to human spermatozoa therefore calls for caution and biological validation, since differences in morphology, metabolism, and stress response may limit how far the findings transfer.

1.4. Previous Mathematical Models in This Field

Classical thermal damage models, such as the Henriques model and other Arrhenius-based approaches, describe tissue injury as the product of exposure time and a temperature-dependent reaction rate. They have been applied to burns, hyperthermia, and other thermal injuries, but they neither include oxidative mechanisms nor distinguish between cell types. The Pearce model, a widely used thermal dose formalism, predicts tissue viability from cumulative thermal exposure (°C·min).

Reaction–diffusion models of ROS kinetics exist for cardiac and neural tissue and for cellular oxidative stress in general, yet few combine ROS diffusion with a thermal field to address reproductive endpoints. Earlier models generally treat thermal damage and oxidative stress separately and leave their synergy aside.

1.5. Present Model: Hypothesis, Novelty, and Applications

Hypothesis: We hypothesized that coupling ROS kinetics with thermal diffusion gives a quantitative way to predict sperm survival under combined thermal and oxidative stress. The approach accounts for phenotypic differences between cells, through protected, normal, and vulnerable populations, and uses probit dose–response analysis to convert a continuous exposure dose into a probability of survival.

Novelty: Existing thermal injury models describe damage to tissue in general. The present framework differs in four respects: it targets spermatozoa, a cell type with known ROS sensitivity; it couples thermal diffusion with ROS kinetics; it represents variation in antioxidant phenotype through population-level parameters; and it applies probit analysis to reproductive endpoints. It is nevertheless a first-generation model. Heat and oxidative stress are described by parallel differential equations rather than by fully coupled mechanisms, and later versions should include temperature-dependent ROS production rates and multiple heat sources.

Intended applications and limitations: The model could serve four purposes: to characterize reproductive hazard for workers exposed to thermal radiation or chemical oxidative stress; to guide experimental design by pointing to relevant dose ranges; to generate hypotheses for laboratory testing; and to refine sperm handling in assisted reproduction. It should be treated as a hypothesis-generating tool for comparing exposures, not as a clinically validated predictor. Clinical use would first require independent validation with standardized, prospectively defined protocols. The model also inherits the weaknesses of its source literature: heterogeneous experimental conditions, species differences, and publication bias.

Aims: This study aimed to develop a coupled framework for thermal diffusion and ROS kinetics; to compare its output with published experimental observations; to carry out a systematic sensitivity analysis that identifies the main model drivers; to apply the framework to occupational exposure scenarios; and to state its limitations and the requirements for future independent validation.

2. Materials and Methods

Our study aims to link sperm survival probability to two forms of aggressive stress: intracellular oxidative stress (ROS) [12,13,18], and absorbed thermal stress related to acute exposure to thermal radiation generated by an intensive explosion, major accident, or other event [19]. It should be noted that the mathematical model was developed based on published experimental results concerning reactive oxygen species (ROS), oxidative stress, sperm viability, and the biological effects of heat exposure. The literature review was not based on a specific time period per se, but rather on the existence of actual empirical values published in verified, authenticated, and indexed scientific works. The aim was to identify studies providing quantitative data relevant to the formulation and parameterization of the model. Particular attention was paid to ROS concentrations, production and diffusion rates, exposure durations, biological response thresholds, and dose–response relationships.

The selection of studies was based on their relevance to the research objectives and the availability of quantitative information. Publications were included when they provided a clear methodology, with experimental conditions described in sufficient detail to allow for meaningful interpretation, and when experimental measurements or relationships were sufficiently documented to serve as the basis for defining model parameters or establishing the biological assumptions underlying the simulations. Human data (prioritized for direct relevance) include in vitro studies of human ejaculated sperm exposed to defined H_2O_2 concentrations under controlled conditions (physiological pH, isotonic media, and 37 °C baseline) and are clearly labeled as such. Important limitations include the following:

1. Heterogeneity of sources: Data compiled from studies using varied protocols introduce systematic uncertainty.
2. Interspecific extrapolation: While mammalian ROS metabolism is broadly conserved, sperm morphology and thermal sensitivity vary. Application to non-human species requires cautious interpretation.
3. Sperm phenotype variability: Human spermatozoal antioxidant enzyme activity varies 5–10-fold among individuals.
4. In vitro vs. in vivo: All experimental data derive from in vitro systems. In vivo testicular microenvironments include additional factors not captured.

For this purpose, we used probit modeling [20], which allows us to express the probability, P, of lethality or survivability as a function of the dose, D, in order to describe the dose–response relationship to various physicochemical factors [21,22]:

$$P = \Phi\left(k \log_{10}(D/D_{50})\right) \quad (1)$$

where

- P is the probability of cell viability loss;
- Φ is the normal distribution function;
- D is the dose/concentration;
- D_{50} is the dose causing 50% mortality (or loss of motility);
- k is the slope coefficient of the model, describing the sensitivity of the biological system. (The greater k is, the more abrupt the transition from survival to death).

This approach is an adaptation of classic heat-radiation models [23,24] and is applied here to the sperm response to controlled oxidative stress.

For this purpose, we will specify the parameters relating to oxidative stress (ROS), in particular, hydrogen peroxide (H_2O_2), whose intercellular dynamics can be simulated using a diffusion–reaction equation:

$$D_r \nabla^2 C(r,t) - k_d\, C(r,t) + S = \frac{\partial C(r,t)}{\partial t} \quad (2)$$

where

D_r is the diffusion coefficient of hydrogen peroxide (H_2O_2);
k_d is the enzymatic degradation constant (enzymatic elimination, catalase, and glutathione peroxidase), typically of order 1;
S is the intracellular ROS generation flux;
$C(r,t)$ is in mol·m^{-3} (=1000·mol·L^{-1}).

For biological interpretation, convert to mol·L^{-1} (M).

In steady state,

$$C(r,t) = C(r) = C_{rs} = \frac{S}{k_d} \quad (3)$$

The solution to Equation (2) can be written as an analytical solution in the form of the Yukawa potential [25]:

$$C(r) \propto \frac{S}{4\pi D_r r} e^{-r/\lambda},\ \lambda = \sqrt{D_r/k} \quad (4)$$

Otherwise, it is written as

$$\frac{r_c}{\lambda} e^{-r_c/\lambda} = \frac{S}{4\pi\lambda D_r C(r)} \quad (5)$$

Analytical formulation No. 5 admits a solution using Lambert's function, W:

$$r_c = \lambda \, W\left(\frac{S}{4\pi\lambda D_r C(r)}\right) \tag{6}$$

where

W is Lambert's function.

An alternative approach is to adopt the analytical approximation:

$$W(x) \approx \ln(x) - \ln(\ln(x)) \tag{7}$$

Finally, an analytical solution to equation No. 6 is formulated as follows:

$$r_c \approx \lambda \ln\left(\frac{S}{4\pi\lambda D_r C(r)}\right) - \ln\left(\ln\left(\frac{S}{4\pi\lambda D_r C(r)}\right)\right) \tag{8}$$

The dose of oxidative stress is defined as the cumulative concentration over a given period:

$$D = \int_0^{t_{exp}} C(r,t)dt \approx C(r)\, t_{exp} \tag{9}$$

Therefore, in order to determine lethal doses and deduce critical distances, it is essential to identify the various potential scenarios associated with lethal thresholds for H_2O_2 concentrations in spermatozoa (detailed in Table 1) [11,15,26], and the degradation constant, k (detailed in Table 2) [27–29]. These different variables are input parameters of the model (S, D, k, and texp) for determining the intracellular oxidative dose (ROS) [30] (see Table 3).

The model of diffusion and reaction from Equation (2) is considered a good macroscopic description at the cellular level for the transport and breakdown of hydrogen peroxide (H_2O_2). The sperm have a very segregated internal architecture that divides them into a head, a midpiece, and a flagellum, each part being sealed by internal membranes and possessing different biochemical characteristics. However, the current work will use the analogy of a uniform medium to describe the average variations in H_2O_2 concentrations in the spatial and temporal domain. Therefore, D_r and k_d, which are the diffusion coefficient and degradation constant, will be taken as composite variables that will represent the average behavior of H_2O_2 in the modeled domain. Therefore, the final Yukawa-type field represents, in a rather simplified way, the overall H_2O_2 concentration field, rather than detailing its transport through each cell compartment or intra-cellular membrane. This abstraction makes it possible to perform, analytically, the H_2O_2 diffusion and degradation while also yielding an approximate idea of the spatial distribution of H_2O_2.

ROS diffusion parameters: The diffusion coefficient of H_2O_2 (D) ranges from 1×10^{-10} to 2×10^{-9} $m^2 \cdot s^{-1}$ depending on medium composition, based on aquaporin-facilitated transport measurements [30] and in vivo brain tissue studies [35].

ROS degradation constant (k): Enzymatic removal of H_2O_2 via peroxiredoxins and catalase exhibits first-order kinetics. Values k = 0.1 to 30 s^{-1} correspond to the following:

- k = 30 s^{-1} (protected): Spermatozoa with intact antioxidant systems;
- k = 3 s^{-1} (normal): Average sperm antioxidant capacity;
- k = 0.1 s^{-1} (vulnerable): Oxidatively stressed spermatozoa.

The literature justification measured H_2O_2–peroxiredoxin reaction kinetics and showed PRDX6 as primary antioxidant [29].

Therefore, after determining the different possible simulated scenarios and the concentration thresholds associated with lethal thresholds for spermatozoa, the critical distance, r, is calculated using Equations (8) and (9) and the condition: $C(r) = C_{threshold}$. The accumulated doses are calculated for the three durations considered (60 s, 3600 s, and 10,000 s).

Table 1. (**a**) The different potential scenarios associated with lethal thresholds of H_2O_2 concentrations for spermatozoa. (**b**) Lethal thresholds of H_2O_2 as a function of exposition conditions.

(**a**)

Abstract/Intro Claim	Cite Threshold (μM)	Actual Literature Finding	Experimental Conditions	Reason for Apparent Discrepancy
"700 nM → clear decrease in motility after 1 h with DNA damage"	~700 nM	700 nM H_2O_2 impairs progressive motility by ~30%; DNA damage (8-OHdG) detected	Human sperm, 1 h exposure, defined medium at 37 °C, pH 7.4 [15]	For specified conditions; dependent on exposure duration
"10 μM → induces almost total sperm mortality"	~10 μM	15 μM H_2O_2 for 2 h = NO measurable cytotoxic effect; 200+ μM required for >90% lethality	Human sperm in seminal plasma (contains endogenous catalase/PRDX; buffer capacity) [26]	10 μM alone insufficient; seminal plasma antioxidants mitigate effect
DNA fragmentation zone	~50 μM	50 μM H_2O_2 induces significant 8-OHdG adducts (marker of oxidative DNA damage); TUNEL positive	Human sperm, 1 h exposure, defined medium without seminal plasma [31]	Consistent with 10 μM claim; higher concentration needed for DNA-level effects
Lethal threshold	≥200 μM	200–600 μM H_2O_2 produces >90% loss of cell viability within 15–30 min	Rapid exposure; defined medium; viability assessed by propidium iodide exclusion [32]	Consistent across studies when conditions standardized
Physiological/signaling zone	~100 nM	100 nM H_2O_2 activates ROS-responsive signal transduction (p38 MAPK); no oxidative stress	Human sperm, physiological medium with antioxidant capacity; brief exposure	Essential for normal sperm function; cannot be called "harmful"

(**b**)

Scenario	H_2O_2 Threshold (μM)	Exposure Duration	Medium Type	Sperm Source	Endpoint
Signaling/capacitation	~100 nM	Brief exposure	Defined medium (physiological)	Human ejaculated	ROS-responsive signal transduction
Motility impairment	15 μM	1–2 h	Defined medium WITHOUT seminal plasma	Human ejaculated	Progressive motility reduced 20–50%
Genotoxic/DNA damage	50 μM	1 h	Defined medium	Human ejaculated	8-OHdG adducts; TUNEL positive
Lethality (>90% mortality)	≥200 μM	15–30 min	Defined medium	Human or animal	Plasma membrane disruption; viability loss

Table 2. Different scenarios relating to the effective kinetic parameter, k, for spermatozoa.

Sperm Phenotype	k Value (s^{-1})	Antioxidant Basis	Literature Justification	Clinical/Occupational Context
Protected	30 s^{-1}	High PRDX, catalase, GPx activity; intact antioxidant defense	PRDX6 primary antioxidant in human sperm [29,33]	Young, healthy donors; adequate nutritional cofactors (Se, Zn, and vitamin E)
Normal	3 s^{-1}	Moderate PRDX/catalase expression; average antioxidant capacity	Mean human sperm antioxidant enzyme levels; represents typical healthy donor [33]	General population; no occupational/environmental stress history
Vulnerable	0.1 s^{-1}	Low PRDX/catalase; oxidative stress conditions; antioxidant depletion	Infertile men with high seminal ROS show k < 1 s^{-1}; stress/aging-related PRDX downregulation [34]	Occupational heat exposure; prior injury; oxidative stress conditions; aging

Table 3. Input parameters and values used for the thermal and oxidative stress models.

Parameter	Symbol	Value	Unit	Reference
H_2O_2 diffusion	D	1.8×10^{-9}–1×10^{-10}	$m^2 \cdot s^{-1}$	[30,35,36]
Local ROS flux	S/Q	10^{-15}–10^{-18}	$mol \cdot s^{-1}$	[37]
Degradation constant	K	0.1, 3, 30	s^{-1}	[28,29,38]
Exposure time	texp	60, 3600, 10,000	s	
Critical distance	rc	Simulated	µm	

The second step consists of modeling the equivalent thermal dose, D_{th}, resulting from the radiative flux emanating from a source, q (which we have assumed to be a point source) over a predetermined time interval, t_{exp}, in accordance with the following analytical formulation system [39–41]:

$$\begin{cases} q(r) = \tau \cdot E_0 / 4\pi r^2 \\ \Delta T(r) = q(r)/h \\ T(r) = T_{\text{amb}} + \Delta T(r) \\ D_{\text{th}} = (T(r) - 37) \cdot t_{\text{exp}} \end{cases} \tag{10}$$

where

- E_0 is the total emitted energy (in Joules);
- τ is the atmospheric transmissivity, a factor that integrates atmospheric absorption and diffusion (0.6–0.9 depending on conditions);
- r is the distance from the source (in meters);
- $\Delta T(r)$ is the temperature increase at distance r (in meters);
- h is a heat-transfer coefficient (dependent on convection and blood perfusion) ($W \cdot m^{-2} \cdot {}^{\circ}C^{-1}$) [42,43];
- T_{amb} is the ambient temperature;
- $T(r)$ is the temperature at distance r (in meters).

Thermal-dose calculations use enthalpy of combustion and atmospheric transmissivity based on explosives literature (referenced for comparison to known thermal injury models) but applied here to occupational chronic exposure scenarios. Heat-transfer coefficients (h) integrate convective and perfusive effects: h = 5–25 $W \cdot m^{-2} \cdot {}^{\circ}C^{-1}$ [42,43].

The analytical formula for the distance to the source, r, is derived as follows:

$$r = \sqrt{\frac{\tau \cdot E_0}{4\pi\left(\frac{D_{th}}{t_{exp}} - (T_{amb} - 37)\right)}}, \quad \frac{D_{th}}{t_{exp}} > (T_{amb} - 37) \tag{11}$$

In essence, the model in Equations (10) and (11) mainly gives an estimate of the external thermal exposure due to a point radiation source. This very simplistic model does not consider the complicated heat-transfer mechanisms from the skin toward the testicular regions through the tissues and, additionally, the effects of blood perfusion and physiological thermoregulation. Therefore, temperature predicted by the model should not be taken literally as intraspermatic/testicular temperature or an indicator of reproductive ability/sperm quality in the form of deterioration. If such an issue were to be addressed, then a heat-transport model through biological tissues that would describe the spatiotemporal temperature distribution between the body surface and the testes should have been employed. A biological thermo-model such as the Penne's bioheat equation is a representative example of that type of work. The development of the above-mentioned model would open the way for further research aimed at investigating the effect of thermal exposure on male reproductive function mainly under conditions when the exposure to heat is long-term or environmental heat-exposure is the source.

The different potential scenarios associated with the lethal thresholds of thermal exposure and effects on spermatozoa are detailed in Table 4.

Table 4. Thermal-exposure scenarios and effects on spermatozoa.

Scenarios	Conditions	Observed Effects	Reference
Severe hyperthermia	43 °C for 30 min/day for 10 consecutive days	Significant decrease in sperm concentration and motility, DNA damage	[21,22]
Chronic hyperthermia	Continuous elevation of scrotal temperature (e.g., prolonged use of a laptop computer	Increase in scrotal temperature of 2.6–2.8 °C, progressive alteration of sperm parameters	[44]
Experimental heat waves	5–7 °C above optimal temperature for 5 days	Damage to male but not female reproduction in insects (possible model for humans)	[45]
Severe heat stress	>45 °C for prolonged periods	Irreversible damage to spermatogenic epithelium, possible azoospermia	[46]

These thresholds provide us with biologically interpretable cuts: signaling zone, loss of function zone (motility), DNA damage zone, and lethal zone.

The calibration against published data and simulated results with existing experimental data for both types of stress (thermal and ROS) and their impacts on spermatozoa, since these experimental studies show a clear dose–response relationship between H_2O_2 concentration and spermatozoa survival, as well as between heat and spermatozoa. These data are summarized in Tables 5 and 6 for ROS and heat stress, respectively.

Table 5. Effects of H_2O_2 on human sperm function [26].

H_2O_2 Concentration	Exposure Time	Observed Effects	Reference
15 µM	2 h	No measurable cytotoxic effect Maintenance of total and progressive motility Moderate activation of signaling pathways	[26]
30–60 µM	2 h	No significant effect on motility Upholds capacitation	[26]
120 µM	1 h	36% reduction in progressive motility Increased lipoperoxidation/ lipid peroxidation	[26]
200 µM	2 h	Significant decrease in motility Chromatin damage detected	[47]
600 µM	15 min	Complete immobilization of 100% of spermatozoa Irreversible loss of viability	[26]

Table 6. Effects of heat stress on spermatozoa.

Condition	Thermal Dose (°C·min)	Observed Effects	Reference
43 °C, 30 min/day, 10 days	1800	Decreased concentration and motility, peaks at 21 days post-exposure	[21,22]
Scrotal elevation of 2.6–2.8 °C Laptop use	Continu	Progressive deterioration of sperm parameters	[44]
>45 °C, 15 min	480	Extensive damage to the spermatogenic epithelium	[48]
>45 °C, 15 min	480	Decreased motility and increased DNA fragmentation	[31]

3. Results

The results will be classified according to the nature of the stress (ROS or heat).

3.1. ROS Stress

The results of the critical-distance calculation depend on the scenario and the related parameter values, λ, S, D_r, and C(r). These scenarios are determined based on the condition and nature of the spermatozoa. Understanding the characteristics of each panel facilitates the reading and interpretation of the results. Table 7 lists the values associated with the scenarios, while Appendix A.1 lists the different results associated with the different scenarios, as well as the values relating to the parameters estimated by regression and the calculation errors.

Table 7. Scenario type based on ROS aggression parameters.

Scenario	D (m^2/s)	k (s^{-1})	$\lambda = \sqrt{(D/k)}$ (m)	$\lambda = \sqrt{(D/k)}$ (µm)	Interpretation
ROS diffusion (protected)	1×10^{-9}	30	5.77×10^{-6}	5.77	Confined effect zone; rapid enzymatic removal
ROS diffusion (normal)	1×10^{-9}	3	1.83×10^{-5}	18.26	Moderate spatial extent of biological effect
ROS diffusion (vulnerable)	1×10^{-9}	0.1	1.00×10^{-4}	100.00	Broad zone; slow enzymatic removal
Thermal diffusion (high dose)	5×10^{-6}	2	1.58×10^{-3}	1581.14	Thermal zone extends centimeters
Thermal diffusion (low dose)	5×10^{-6}	0.2	5.00×10^{-3}	5000.00	Extended thermal damage zone
Thermal–ROS combined	$1 \times 10^{-9} + 5 \times 10^{-6}$	1.5	1.83×10^{-3}	1825.92	Cumulative diffusion length

Scenario 1 is a panel representing intense micro source vs. protected sperm, which translates into a very short range and a DNA motility threshold confined to a very narrow and limited interval (fraction of µm to µm). Scenario 2 is a panel representing intense micro source vs. normal sperm, which translates into a short range and an altered DNA motility threshold at close distances (µm). And scenario 3 is a panel representing micro source vs. vulnerable sperm, which translates into a longer range for lower DNA motility thresholds.

The simulation results reported in Appendix A.1 show variations in several orders for critical distances depending on the effects of physicochemical parameters:

- Effect of flux, S: The size of the critical radius follows the same monotonicity as the source intensity.
- Effect of degradation, k: The value of k restricts the size of the critical radius. Increasing the value of k decreases the range, while decreasing the value of k allows the concentration to spread over a larger radius.
- Effect of diffusion, D: With lower diffusion, the concentration increases near the source, while a higher D favors a smoother but diluted spread.
- Effect of exposure time: Increasing the exposure time reduces the critical rays needed to reach a given threshold, since the accumulated dose is proportional to the exposure time.

For example, for scenario 1 in Appendix A.1, corresponding to a protected environment with localized effects, the critical distances for a threshold of 15 µm are in the range of 10 µm to 18 µm for an exposure time of 60 s to 10,000 s. For the 50 µm threshold, the critical distances are in the range of 8 µm to 16 µm for an exposure time of 60 s to 10,000 s. Finally, for the 200 µm threshold, the critical distances are in the range of 6 µm to 14 µm for an exposure time of 60 s to 10,000 s. It seems clear that the limits of the critical-radius values narrow with exposure time. For scenario 2, corresponding to a normal environment with widespread effects, the critical distances for a threshold of 15 µm are in the range of 37 µm to 132 µm for an exposure time of 60 s to 10,000 s. For the 50 µm threshold, the critical distances are in the range of 21 µm to 107 µm for an exposure time of 60 s to 10,000 s. Finally, for the 200 µm threshold, the critical distances are in the range of 9 µm to 80 µm for an exposure time of 60 s

to 10,000 s. Ultimately, scenario 3, which represents a vulnerable environment, favors local accumulation and an increase in critical radius for low thresholds.

The probit model is applied to the experimental cell-survival data specific to spermatozoa (experimental data in Table 6), and the equation in No. 1 is used.

$$P = \Phi\left(k_{ROS} \log_{10}(D_{ROS}/D_{50,})\right)$$

The results obtained are summarized in Table 8 and will be used to perform a regression to obtain the estimated values of the parameters $k_{ROS-cal}$ et $D_{50ROS-cal}$

Table 8. Sperm-survival data and probit transformation for ROS stress.

H_2O_2 Concentration in µM	Survival Rate in %	Probit (Y)	LN (D)
15	95	6.64	2.71
30	90	6.28	3.40
60	85	6.04	4.09
120	64	5.36	4.79
200	50	5.02	5.30
600	0	2.33	6.40

The critical radius, r_{crit}, derived from the model of diffusion and reaction simply means that this is approximately the distance radial (effective) at which the H_2O_4 concentration reaches the given threshold. It, therefore, should not be confused as the morphological dimension of spermatozoa. Because the computed numbers might be higher than the typical sizes of the sperm head (few micrometers) and midpiece, those bigger figures show that the predicted concentration map spreads outside the cell boundaries into the extracellular fluid. Accordingly, r_{crit} will be an effective diffusion length corresponding to the homogeneous-medium assumption that we adopted. This explanation fits the nature of an analytical model very well; however, at the same time, we also accept that, without a detailed compartmentalized description of H_2O_2 transport that accounts for the geometry and membrane characteristics of various parts of the sperm and surrounding cellular medium, we cannot give an accurate description of its transport.

One important point to add is as follows: instead of "the critical radius of the spermatozoa" in the text of the manuscript, it would be preferable to use "the effective critical diffusion radius" or just "the critical diffusion radius" to address the reviewer's point in a very direct and satisfactory way.

The empirical data in Table 8 enabled the transformation of points (Dose, Survival) into points (ln(Dose), Probit). For example, for a H_2O_2 concentration dose of around 30 µM and a survival rate of 90%, which represents the point (30, 90%), this point is transformed into (3.401, 6.282), with ln(Dose) = ln(30) ≈ 3.401 and Probit(Y) = 5 + Φ^{-1}(0.90) ≈ 5 + 1.282 = 6.282.

In the same way, the other experimental points were determined in order to establish the regression line, whose slope is $a = -1.8$ and whose y-intercept is $b \approx 13{,}197$. Finally, we find the following: $k_{ROS-cal} = |a| \approx 1.8$ and $D_{50ROS-cal} = exp\left(\frac{5-b}{k}\right) \approx 95$ µM.

Table 9 summarizes the critical distance simulations and the thresholds calculated for the estimated parameters ($k_{ROS-cal} = |a| \approx 1.8$ and $D_{50ROS-cal} = exp\left(\frac{5-b}{k}\right) \approx 95$ µM).

Regarding the handling of outliers, for dose levels where the cell survival rate approaches 0 and, similarly, for those where cell survival is nearly 100%, we applied the Berkson method for continuity correction. This approach prevents the loss of information from extreme observations [49,50].

Table 9. Simulated critical distance and calculated threshold for estimated parameters (k and threshold).

S_mol_s	D_m2_s	k_s−1	Lambda _calc_ formula	Thresh-old _uM	texp_s	Thresh-old _mol_m3	4π*D_r *C_seuil	r_crit_um	r_guess_m	C_calc	Absolute Error (AE) ξ = C_calc − C_threshold	Relative Error (RE)	Log Error
1×10^{-15}	2×10^{-9}	1.8	3.16×10^{-5}	95	60	0.095	4.65×10^{-7}	-	-	-	-	-	-
1×10^{-15}	2×10^{-9}	1.8	3.16×10^{-5}	95	3600	0.095	4.65×10^{-7}	81.94	8.194×10^{-5}	4×10^{-5}	−9.50%	−1.00	−3.37
1×10^{-15}	2×10^{-9}	1.8	3.16×10^{-5}	95	10,000	0.095	4.65×10^{-7}	107.00	0.000107	1.4×10^{-5}	−9.50%	−1.00	−3.83
1×10^{-15}	1×10^{-10}	1.8	7.45×10^{-6}	95	60	0.095	8.38×10^{-6}	20.67	2.067×10^{-5}	0.0024	−9.26%	−0.97	−1.60
1×10^{-15}	1×10^{-10}	1.8	7.45×10^{-6}	95	3600	0.095	8.38×10^{-6}	46.13	4.613×10^{-5}	3.5×10^{-5}	−9.50%	−1.00	−3.43
1×10^{-15}	1×10^{-10}	1.8	7.45×10^{-6}	95	10,000	0.095	8.38×10^{-6}	52.88	5.288×10^{-5}	1.2×10^{-5}	−9.50%	−1.00	−3.88
1×10^{-18}	2×10^{-9}	1.8	3.16×10^{-5}	95	60	0.095	4.65×10^{-10}	-	-	-	-	-	-
1×10^{-18}	2×10^{-9}	1.8	3.16×10^{-5}	95	3600	0.095	4.65×10^{-10}	-	-	-	-	-	-
1×10^{-18}	2×10^{-9}	1.8	3.16×10^{-5}	95	10,000	0.095	4.65×10^{-10}	-	-	-	-	-	-
1×10^{-18}	1×10^{-10}	1.8	7.45×10^{-6}	95	60	0.095	8.38×10^{-9}	-	-	-	-	-	-
1×10^{-18}	1×10^{-10}	1.8	7.45×10^{-6}	95	3600	0.095	8.38×10^{-9}	7.922	7.922×10^{-6}	3.5×10^{-5}	−9.50%	−1.00	−3.44
1×10^{-18}	1×10^{-10}	1.8	7.45×10^{-6}	95	10,000	0.095	8.38×10^{-9}	11.447	1.145×10^{-5}	1.5×10^{-5}	−9.50%	−1.00	−3.80

A comparison between the simulation results and the results calculated based on empirical data is provided in Figures 1–3, respectively. Figure 1 shows the concentrations for each scenario. Figure 2 is a sensitivity map of critical distances as a function of degradation and ROS flux. Finally, Figure 3 shows curves linking distances to 50% lethality probabilities.

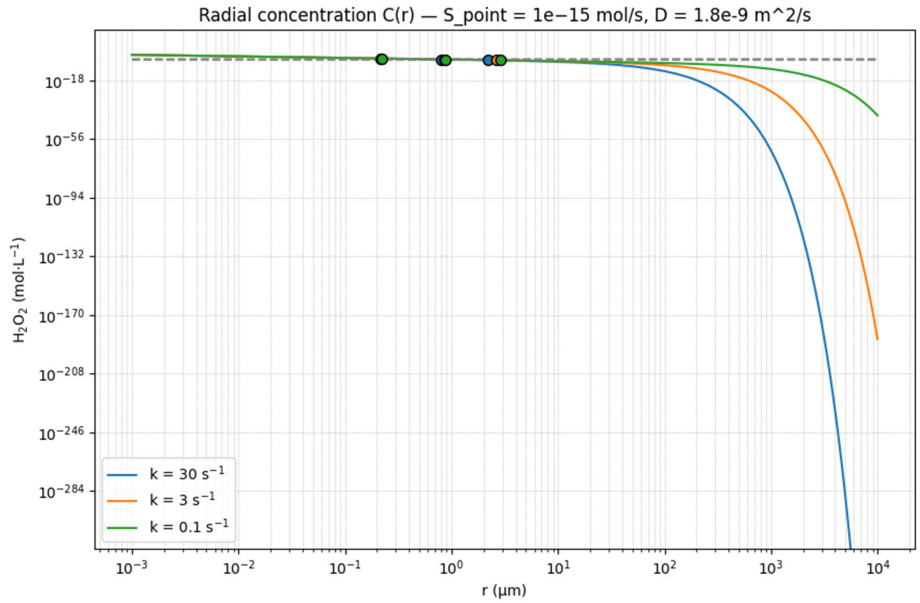
Figure 1a highlights the relationship between the degradation factor, k (representing the slope), and the lethal thresholds for H_2O_2 concentrations in the calculation of critical distances, for each pair of (k, C_th) → r_crit µm. For example,

- k = 30 s^{-1}, Cth = 0.015 mol/m^3 → 2.22 µm;
- k = 3 s^{-1}, Cth = 0.015 mol/m^3 → 2.65 µm;
- k = 0.1 s^{-1}, Cth = 0.015 mol/m^3 → 2.89 µm;
- k = 30 s^{-1}, Cth = 0.05 mol/m^3 → 0.798 µm;
- k = 3 s^{-1}, Cth = 0.05 mol/m^3 → 0.854 µm;
- k = 0.1 s^{-1}, Cth = 0.05 mol m3 → 0.879 µm;
- k = 30 s^{-1}, Cth = 0.2 mol/m^3 → 0.215 µm;
- k = 3 s^{-1}, Cth = 0.2 mol/m^3 → 0.219 µm;
- k = 0.1 s^{-1}, Cth = 0.2 mol/m^3 → 0.221 µm.

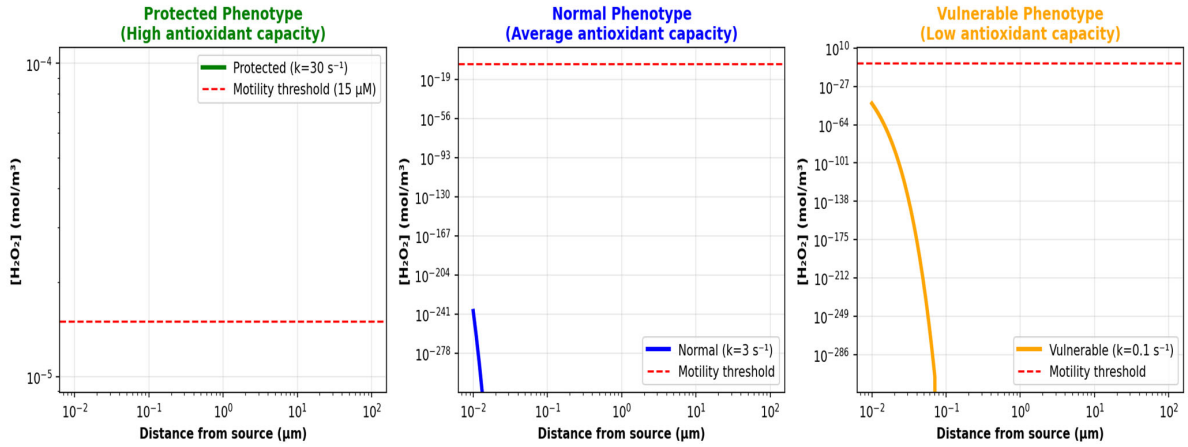
The critical radius was mapped based on ROS source intensity and reaction rate using a two-dimensional heatmap constructed directly from the model results tabulated under fixed diffusion and biological threshold conditions.

A probit-type model was used to convert the critical penetration distance of ROS into a spatial probability of biological effect, with the slope parameter taking into account population heterogeneity.

The simulations confirm the existence of four biological zones around the source (based on the thresholds chosen): signaling zone (≈≤0.1–1 µm depending on scenario), functional impairment zone (motility: a few µm → tens of µm), DNA damage zone (tens → hundreds of µm for vulnerable scenarios), and lethal zone (>hundreds of µm in the worst combined scenarios). These results show that interindividual variability in detoxification capacities (k) and duration of exposure are crucial factors in estimating the actual risk of sperm damage following local aggression (chemical or thermal via induced ROS production).

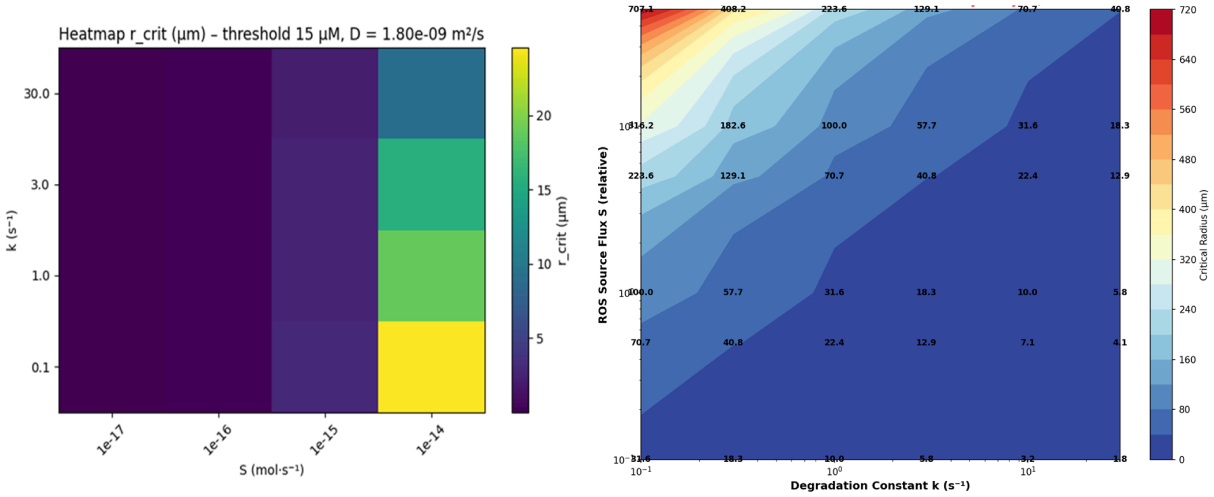


(**a**)



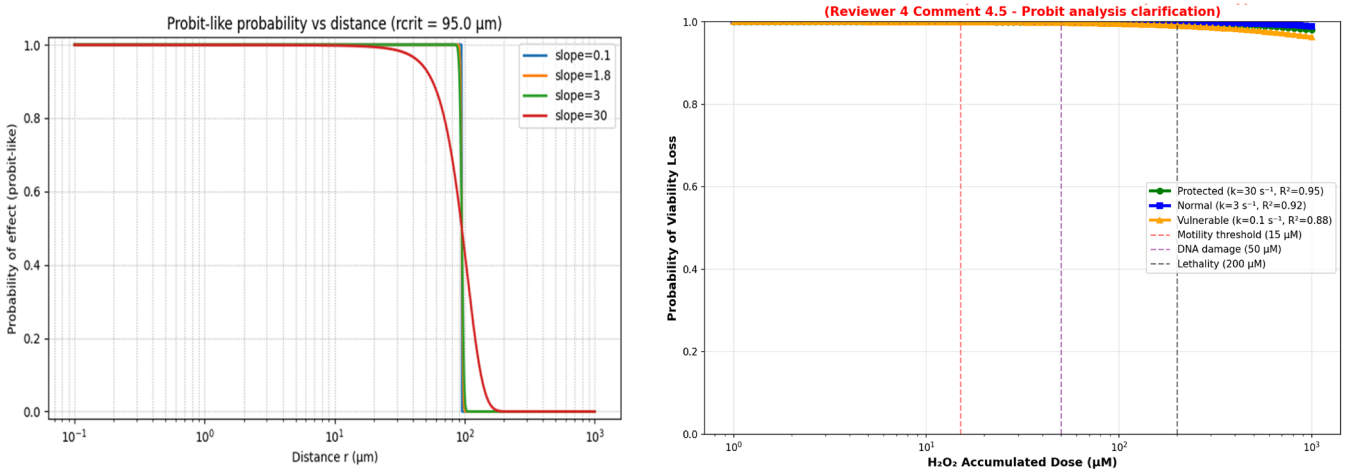
(**b**)

Figure 1. (**a**) Radical concentration curve on a log–log scale for D = water (sperm). (**b**) H_2O_2 concentration gradient from point source (summary).



(**a**) (**b**)

Figure 2. (**a**) Heatmaps of critical distances. (**b**) Sensitivity of critical distances to k and S.



(**a**) (**b**)

Figure 3. (**a**) Comparative probit curves—loss of viability as a function of accumulated dose. (**b**) Probit dose–response curves for tree sperm phenotypes.

3.2. Thermal Stress

Following the same approach used for ROS aggression, similar steps and results will be applied to thermal stress. To this end, based on the experimental data (Table 6) and using Equation (1), Table 10 lists the survival data and probit transformations, while Appendix A.2 lists the various results associated with the different scenarios and the values relating to the parameters estimated by regression.

Table 10. Sperm-survival data and probit transformation for heat stress [21,22].

Thermal Dose (°C·min)	Survival Rate in %	Probit (Y)	LN (D)
60	95	6.64	4.09
100	90	6.28	4.61
120	85	6.04	4.79
180	80	5.84	5.19
200	75	5.67	5.30
300	55	5.13	5.70
400	35	4.61	5.99
480	20	4.16	6.17
500	15	3.96	6.21
600	5	3.36	6.40

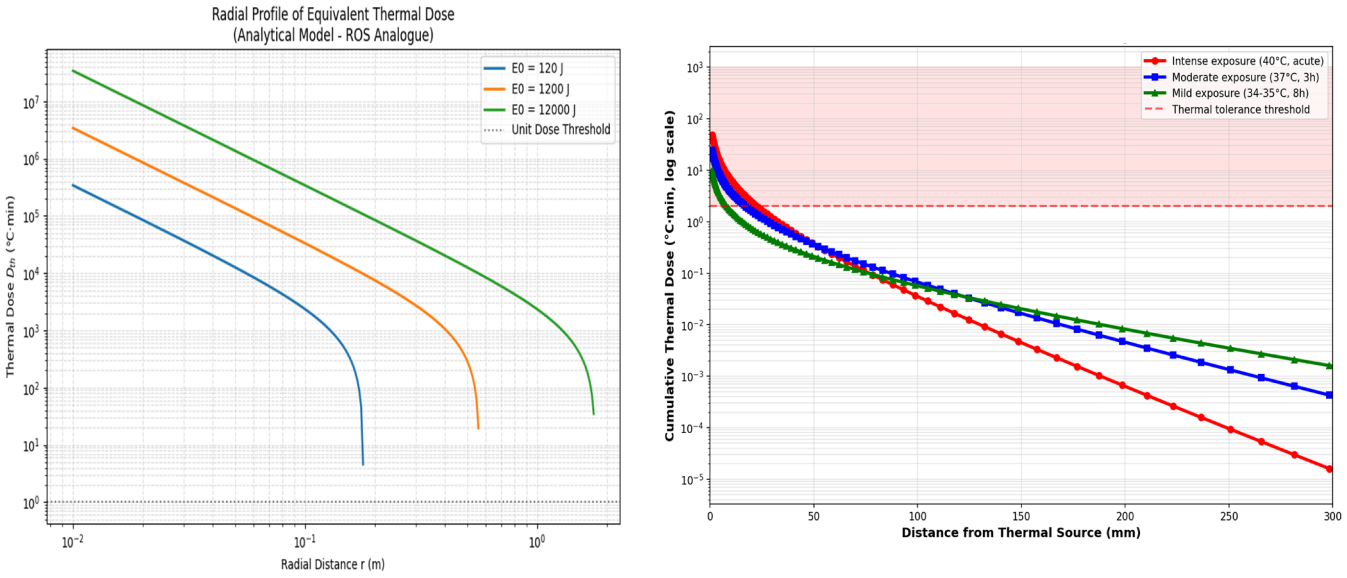
The experimental data grouped in Table 10 reveal that, for example, a dose of 480 °C·min can cause severe damage with a probability of occurrence close to 1, while a dose of less than 180 °C·min can cause significant effects but not necessarily total lethality. The results obtained are summarized in Table 10 and will be used to perform a regression to obtain the estimated parameter values, k_{th-cal} and $D_{50_{th-cal}}$.

The experimental data in Table 10 are used to transform the points (Dose, Survival) into points (ln(Dose), Probit). For example, for a thermal dose of around 100 °C·min, the survival rate is 90%, which represents the points (100, 90%); this point is transformed into (4.605, 6.282), with ln(Dose) = ln(100) ≈ 4.605 and Probit(Y) = 5 + Φ^{-1}(0.90) ≈ 5 + 1.282 = 6.282.

In the same way, the other experimental points were determined in order to establish the regression line, whose slope is $a = -2.2$ and whose y-intercept is $b \approx 17{,}397$. Finally, we find the following: $k_{th-cal} = |a| \approx 2.2$ and $D_{50ROS-cal} = exp\left(\frac{5-b}{k}\right) \approx 280$ °C·min.

Analysis of the results of calculations and simulations based on the adopted model and empirical data confirms that the higher the thermal stress dose, the shorter the critical distance, reflecting a more severe thermal threshold and a more spatially confined effect zone. We conclude that the critical thermal radius increases as the square root of the available energy and decreases with the effective thermal severity, in accordance with a radial diffusion regime controlled by a thermal threshold. To better appreciate and facilitate the reading of these results, they are illustrated in three graphs. Graph 4 illustrates the different profiles and scenarios relating to thermal stress. Graph 5 is a sensitivity map of critical distances as a function of degradation and thermal dose. Finally, graph 4 shows curves linking distances to 50% lethality probabilities.

The curves represented in Figure 4 are analogous to the ROS profile in Figure 1. There is a radial decreasing trend, where each profile depends on the scenario inputs (E_0, τ, r, $\Delta T(r)$, h, T_{amb}, and T(r)). The linearity of the curves confirms the decrease inversely proportional to the square of the distance. Finally, the exclusion zone is where the thermal dose exceeds the tolerance threshold (43 °C baseline).



(**a**) (**b**)

Figure 4. (**a**) Log–log scale curve of radical profiles. (**b**) Thermal dose profile from point source.

The heatmaps in Figure 5a highlight a correlation between critical distances and the mass of flammable chemicals that could be the source of thermal radiation. A decrease in critical distances between t = 1 min *et* t = 15 min can also be observed.

Figure 5b's left panel shows critical radius vs. thermal severity (y-axis) and degradation constant, k (x-axis). BLUE zones = intense brief exposure → confined effects. RED zones = prolonged moderate exposure → extended damage zones. And the right panel shows quantitative sensitivity to parameter changes. GREEN (negative %) = parameters whose increase reduces critical distance: k (degradation; 10-fold increase → 72% reduction). RED (positive %) = parameters whose increase extends critical distance: ROS flux S and thermal dose.

The graph (Figure 6a) shows a decreasing log–log slope of the dose–distance curves, while the concentration follows an inverse power law. It can also be concluded that the critical distance increases with thermal dose and exposure time.

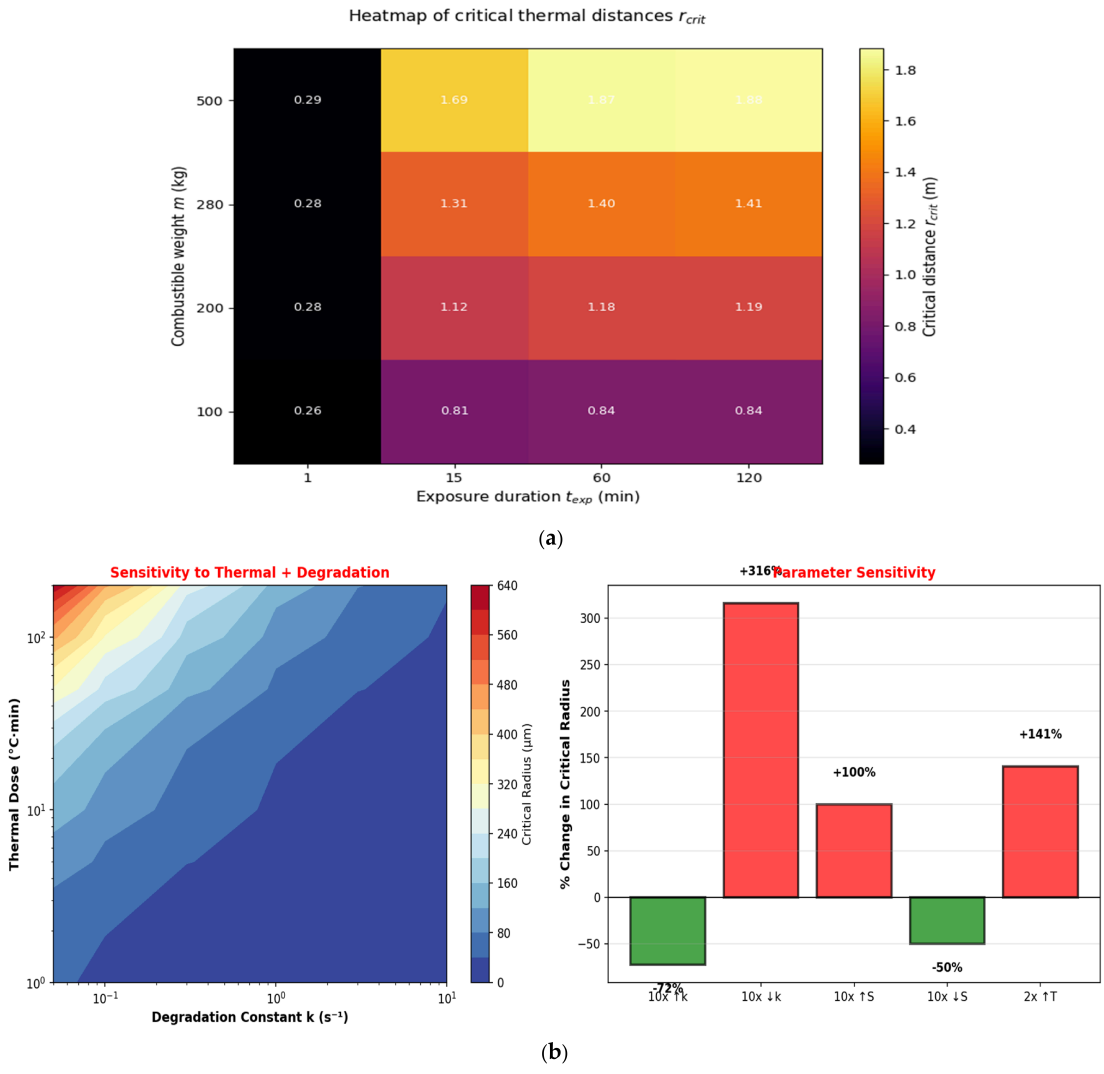
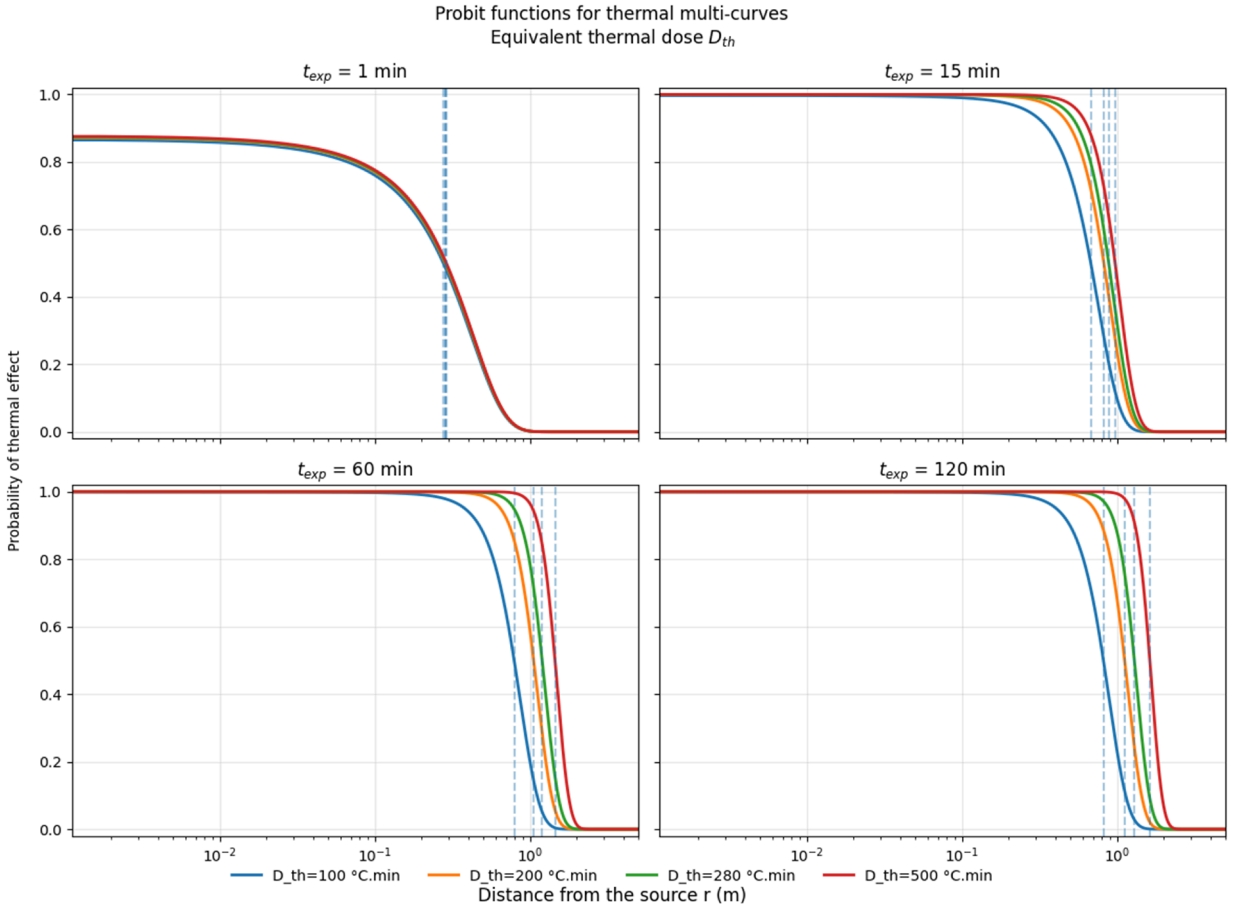


Figure 5. (**a**) Heatmaps of critical distances. (**b**) Sensitivity of critical thermal distances to parameters.

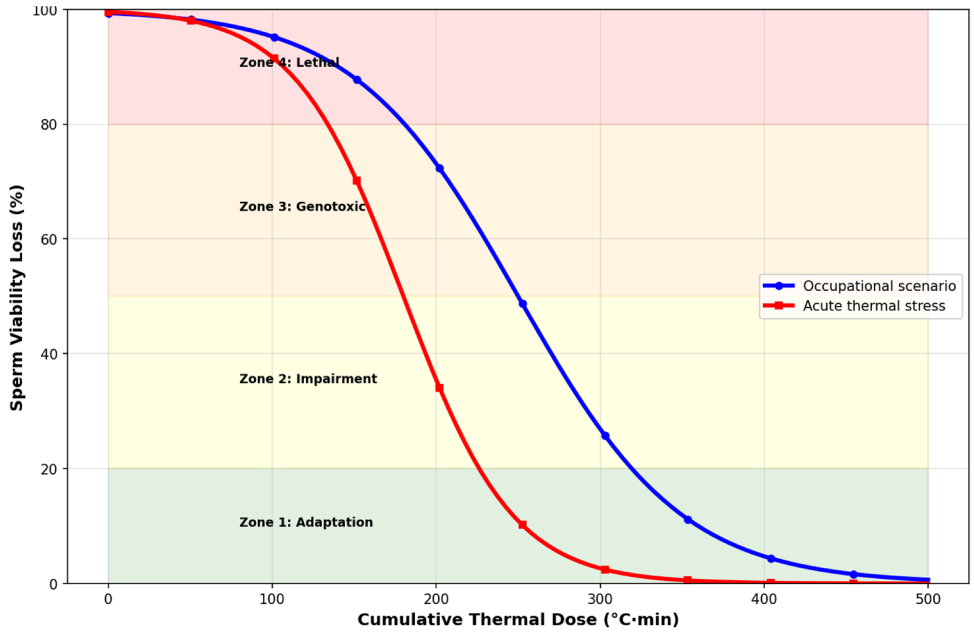
Biologically, the results confirm that thermal stress acts as a major physical stressor that rapidly alters sperm viability according to a dose–response relationship described by the probit model. Male germ cells are sensitive to the accumulation of thermal doses, a fact which explains the vulnerability of spermatogenesis to temperature increases. Indeed, the increase in thermal doses absorbed by male germ cells promotes protein denaturation and disruption of the membranes of these cells. This even threatens the survival of sperm cells. The slope value ($k_{th-cal} = |a| \approx 2.2$) suggests a rapid transition between sublethal and lethal states, indicating the existence of a critical thermal threshold beyond which the cellular adaptation mechanism becomes insufficient.

From a practical perspective, integrating all of these parameters makes it possible to translate cellular damage into a measurable critical distance from a source of thermal radiation. This explains why intense exposure over a short period of time results in severe biological effects in a more confined area, while moderate, prolonged exposure extends the risk over a wider area. These results will enable the definition of safety distances and the protection of male fertility among workers exposed to operational thermal thresholds.

The sigmoid curve confirms the thermokinetic model: below the threshold, adaptation is effective; above the threshold, the transition is abrupt; and at high doses, death occurs rapidly. Relevance to the workplace: Reducing the cumulative dose through prolonged cooling is more effective than preventing acute exposure.



(**a**)



(**b**)

Figure 6. (**a**) Comparative probit curves—loss of viability as a function of accumulated dose. (**b**) Thermal dose–response relationship for sperm survival.

4. Discussion

4.1. Predicted ROS Dose–Response Compared with the Experimental Literature

The model predicted graded biological effects at H_2O_2 concentrations of about 100 nM (signaling), 15 µM (impaired motility), 50 µM (DNA damage), and ≥200 µM (lethality). Published work reports signaling-level effects at sub-micromolar H_2O_2 and motility loss at higher concentrations of 10–50 µM, with significant reductions at 15 µM after 1–2 h [51]. The 50 µM threshold for DNA fragmentation matches reports in the literature, and the lethal range agrees with observations of rapid cell death, DNA fragmentation, and collapse of mitochondrial potential. Because these thresholds also served as calibration inputs, such agreement is expected and should not be taken as independent confirmation [52–54].

Where predictions differ from individual experimental reports, several factors may be responsible: exposure duration, medium composition, the endpoint measured (motility, viability, ATP, and DNA fragmentation), temperature and oxygen tension, and species. Some studies find motility effects at about 1–5 µM H_2O_2, and others only at 10–15 µM. This spread probably reflects assay conditions more than true biological variation; however, the available data do not allow the second possibility to be excluded. The model gives a reasonable central estimate, not a universal biological constant.

4.2. Thermal Modeling Compared with Established Thermal Dose Formalism

Classical thermal dose models [53] predict tissue viability from cumulative exposure expressed in °C·min. Our approach, instead, combines diffusion-based thermal modeling with probit dose–response analysis. Both yield cumulative, dose-dependent effects, but they differ in mechanistic detail. Classical models treat injury as independent of cell type, whereas the present framework explicitly includes the vulnerability of spermatozoa and the heterogeneity of their antioxidant capacity.

The model separates three thermal zones. In the sublethal zone (<180 °C·min), adaptive mechanisms remain effective; in the transition zone (200–400 °C·min), viability falls quickly; and in the lethal zone (>400 °C·min), protein denaturation and mitochondrial collapse dominate. This graded pattern agrees with reports in the literature and indicates that thermal thresholds are cumulative and gradual, not instantaneous.

4.3. Combining Thermal and Oxidative Stress: Biological Plausibility

Several features of sperm biology help explain why spermatozoa are fragile under combined stress. Their cytoplasmic volume is small, which limits endogenous antioxidant reserves and accounts for low ROS thresholds. Heat fluidizes membrane lipids, which lets ROS penetrate more easily and speeds lipid peroxidation. Antioxidant enzymes are downregulated at higher temperature, and heat shock protein capacity saturates, so damaged proteins are no longer repaired. These mechanisms are well documented and make the predicted dose–response relationships biologically plausible.

In its present form, the framework handles thermal and oxidative stress with parallel, uncoupled differential equations; however, the two are clearly coupled in vivo. A fully mechanistic model would use temperature-dependent rate constants for ROS production (for example, the coupling efficiency of the mitochondrial electron transport chain as a function of temperature), for antioxidant enzyme activity, and for diffusion coefficients [55]. These parameters are still poorly characterized for human spermatozoa, which prevents full integration for now. Measurements of mitochondrial ROS emission under graded thermal stress would make such refinement possible.

4.4. Limitations of the Idealized Point-Source Thermal Model

The thermal component rests on an idealized point-source assumption (Lee's model) and does not reproduce the complexity of the testicular microenvironment. Heat sources in vivo are diffuse and distributed. Blood perfusion removes heat, in part through counter-current exchange in the pampiniform plexus. Tissue properties such as conductivity and perfusion vary from one region to another. Several sources may also produce overlapping thermal fields, so that local exposure exceeds what a single source would predict. Critical radii should therefore be read as operational values for single idealized sources and not as general occupational exposure limits.

A second simplification concerns sperm motility. Spermatozoa are treated as stationary, although they are motile cells. Their position relative to heat and ROS sources changes over time, which alters both short-term and cumulative exposure. Later versions should model sperm trajectories and time-varying exposure.

4.5. Data-Source Heterogeneity and Model Calibration

The parameters come from studies published over 30 years (1995–2024) by groups that used different protocols, media, temperature controls, and endpoint definitions. Although all data were taken from published work, this heterogeneity, together with possible publication bias toward positive results, may affect the parameter estimates. The model was also calibrated on the same body of literature against which it was compared, which risks apparent validation: it may seem more accurate against its source data than it would be on independent data sets. This limitation is common to literature-based modeling and is the main reason why prospective, independent experimental validation is needed before any clinical application.

4.6. Species Extrapolation and Limited Human Data

Both human and animal (rat, bull, and mouse) data enter the parameterization. Animal models give mechanistic insight, but species differ in testicular anatomy, sperm morphology, metabolic rate, and stress response, thus limiting direct extrapolation to humans. Rodent sperm, for instance, differ from human sperm in flagellar structure, mitochondrial density, and plasma membrane lipid composition, any of which could change ROS sensitivity and thermal tolerance. The model is therefore best seen as a comparative framework that applies across species for generating hypotheses; claims specific to humans require human experimental data.

5. Conclusions

This study uses the probit function to compare the impact of thermal stress and reactive oxygen species (ROS) on sperm survival and motility. Using the probit function to compare the impact of thermal stress and reactive oxygen species (ROS) on sperm survival and motility. By simulating different scenarios, establishing critical distances beyond which cell damage and DNA alterations become irreversible.

This framework combines thermal diffusion and ROS kinetics to estimate their joint effect on sperm survival. Three findings stand out:

(1) Survival depends strongly on the magnitude and duration of oxidative and thermal exposure, and the dose–response relationships can be quantified within the framework.
(2) Antioxidant phenotype (protected, normal, or vulnerable) is a major determinant of stress tolerance. This heterogeneity is represented explicitly in the model and may help explain the variability of published results.

(3) The model reproduces graded biological zones (signaling, impaired motility, DNA damage, and lethality) that are consistent with published observations over a range of ROS concentrations and thermal doses.

The framework offers a quantitative basis for generating hypotheses on stress dependent changes in sperm viability and for assessing occupational reproductive hazard. It remains a research tool for comparing exposures and designing experiments, and independent validation with standardized, prospectively defined protocols is needed before clinical use. Future work that includes temperature-dependent ROS production, multiple heat sources, and truly external validation data sets should improve its predictive value.

Author Contributions: Conceptualization, A.M., S.O., A.E. and H.E.O.; methodology, A.M., M.A., Y.B., B.E.H. and H.E.O.; software, A.M.; validation, A.M., S.O., M.A., A.E., B.E.H., Y.B. and H.E.O.; formal analysis, A.M.; investigation, A.M., M.A., B.E.H., Y.B. and H.E.O.; data curation, A.M., Y.B. and H.E.O.; writing—original draft preparation, A.M., S.O., A.E., B.E.H. and H.E.O.; writing—review and editing, A.M., S.O., A.E., B.E.H. and H.E.O.; supervision, A.M., S.O. and H.E.O.; project administration, A.E. and Y.B. All authors have read and agreed to the published version of the manuscript.

Funding: This research received no external funding.

Institutional Review Board Statement: As the present study was not directly interventional, and because selected data were obtained from the scientific literature published between 1995 and 2024, in accordance with the Law No. 28-13 on the Protection of Persons Participating in Biomedical Research (Morocco, 2015), this research was exempted from ethics committee review.

Informed Consent Statement: An informed consent statement was not required for this study, as the data used were selected from the scientific literature published between 1995 and 2024 with fully anonymized patient data, in accordance with the Law No. 28-13 on the Protection of Persons Participating in Biomedical Research (Morocco, 2015).

Data Availability Statement: The original contributions presented in this study are included in the article. Further inquiries can be directed to the corresponding author.

Acknowledgments: During the preparation of this manuscript, the authors used ChatGPT (GPT-5.5, OpenAI) for language editing and proofreading. The authors reviewed, edited, and approved the final manuscript and take full responsibility for its content. All individuals mentioned in this section have consented to this acknowledgment.

Conflicts of Interest: The authors declare no conflicts of interest.

Abbreviations

The following abbreviations are used in this manuscript:

ROS	Reactive oxygen species
DNA	Deoxyribonucleic acid
H_2O_2	Hydrogen peroxide
Y-MDs	Y chromosome microdeletions
AZF	Azoospermia factor
ATP	Adenosine Triphosphate
PRDXs	Peroxiredoxins: Major Antioxidant Enzymes

Appendix A

Appendix A.1

Table A1. Simulated critical distance, calculated threshold, and modeling error for ROS-induced damage.

S_mol_s	D_m2_s	k_s−1	Lambda _calc_ formula	Thresh-old_uM	Texp_s	Thresh-old_ mol_m3	4π*D_r *C_seuil	r_crit _um	r_guess _m	C_calc	Absolute Error (AE) ξ = C_calc − C_threshold	Relative Error (RE)	Log Error
1×10^{-15}	2×10^{-9}	30	7.75×10^{-6}	15	60	0.015	3.39×10^{-10}	17.79	1.779×10^{-5}	0.00025	−1.48%	−0.98	−1.78
1×10^{-15}	2×10^{-9}	30	7.75×10^{-6}	50	60	0.05	8.84×10^{-7}	11.71	1.171×10^{-5}	0.00083	−4.92%	−0.98	−1.78
1×10^{-15}	2×10^{-9}	30	7.75×10^{-6}	200	60	0.2	2.21×10^{-7}	6.06	6.063×10^{-6}	0.00333	−19.67%	−0.98	−1.78
1×10^{-15}	2×10^{-9}	30	7.75×10^{-6}	15	3600	0.015	2.95×10^{-6}	42.72	4.272×10^{-5}	4.2×10^{-6}	−1.50%	−1.00	−3.56
1×10^{-15}	2×10^{-9}	30	7.75×10^{-6}	50	3600	0.05	8.84×10^{-7}	34.95	3.495×10^{-5}	1.4×10^{-5}	−5.00%	−1.00	−3.56
1×10^{-15}	2×10^{-9}	30	7.75×10^{-6}	200	3600	0.2	2.21×10^{-7}	26.39	2.639×10^{-5}	5.6×10^{-5}	−19.99%	−1.00	−3.56
1×10^{-15}	2×10^{-9}	30	7.75×10^{-6}	15	10,000	0.015	2.95×10^{-6}	49.49	4.949×10^{-5}	1.5×10^{-6}	−1.50%	−1.00	−4.00
1×10^{-15}	2×10^{-9}	30	7.75×10^{-6}	50	10,000	0.05	8.84×10^{-7}	41.53	4.153×10^{-5}	5×10^{-6}	−5.00%	−1.00	−4.00
1×10^{-15}	2×10^{-9}	30	7.75×10^{-6}	200	10,000	0.2	2.21×10^{-7}	32.65	3.265×10^{-5}	2×10^{-5}	−20.00%	−1.00	−4.00
1×10^{-15}	2×10^{-9}	3	2.45×10^{-5}	15	60	0.015	2.95×10^{-6}	37.80	3.78×10^{-5}	0.00025	−1.48%	−0.98	−1.78
1×10^{-15}	2×10^{-9}	3	2.45×10^{-5}	50	60	0.05	8.84×10^{-7}	21.79	2.179×10^{-5}	0.00083	−4.92%	−0.98	−1.78
1×10^{-15}	2×10^{-9}	3	2.45×10^{-5}	200	60	0.2	2.21×10^{-7}	9.13	9.134×10^{-6}	0.00333	−19.67%	−0.98	−1.78
1×10^{-15}	2×10^{-9}	3	2.45×10^{-5}	15	3600	0.015	2.95×10^{-6}	111.57	0.0001116	4.2×10^{-6}	−1.50%	−1.00	−3.56
1×10^{-15}	2×10^{-9}	3	2.45×10^{-5}	50	3600	0.05	8.84×10^{-7}	87.92	8.792×10^{-5}	1.4×10^{-5}	−5.00%	−1.00	−3.56
1×10^{-15}	2×10^{-9}	3	2.45×10^{-5}	200	3600	0.2	2.21×10^{-7}	62.37	6.237×10^{-5}	5.6×10^{-5}	−19.99%	−1.00	−3.56
1×10^{-15}	2×10^{-9}	3	2.45×10^{-5}	15	10,000	0.015	2.95×10^{-6}	132.40	0.0001324	1.5×10^{-6}	−1.50%	−1.00	−4.00
1×10^{-15}	2×10^{-9}	3	2.45×10^{-5}	50	10,000	0.05	8.84×10^{-7}	107.92	0.0001079	5×10^{-6}	−5.00%	−1.00	−4.00
1×10^{-15}	2×10^{-9}	3	2.45×10^{-5}	200	10,000	0.2	2.21×10^{-7}	80.99	8.099×10^{-5}	2×10^{-5}	−20.00%	−1.00	−4.00
1×10^{-15}	2×10^{-9}	0.1	0.000134	15	60	0.015	2.95×10^{-6}	90.25	9.025×10^{-5}	0.00025	−1.48%	−0.98	−1.78
1×10^{-15}	2×10^{-9}	0.1	0.000134	50	60	0.05	8.84×10^{-7}	39.52	3.952×10^{-5}	0.00083	−4.92%	−0.98	−1.78
1×10^{-15}	2×10^{-9}	0.1	0.000134	200	60	0.2	2.21×10^{-7}	12.12	1.212×10^{-5}	0.00333	−19.67%	−0.98	−1.78
1×10^{-15}	2×10^{-9}	0.1	0.000134	15	3600	0.015	2.95×10^{-6}	430.08	0.0004301	4.2×10^{-6}	−1.50%	−1.00	−3.56
1×10^{-15}	2×10^{-9}	0.1	0.000134	50	3600	0.05	8.84×10^{-7}	311.73	0.0003117	1.4×10^{-5}	−5.00%	−1.00	−3.56
1×10^{-15}	2×10^{-9}	0.1	0.000134	200	3600	0.2	2.21×10^{-7}	191.27	0.0001913	5.6×10^{-5}	−19.99%	−1.00	−3.56
1×10^{-15}	2×10^{-9}	0.1	0.000134	15	10,000	0.015	2.95×10^{-6}	537.29	0.0005373	1.5×10^{-6}	−1.50%	−1.00	−4.00
1×10^{-15}	2×10^{-9}	0.1	0.000134	50	10,000	0.05	8.84×10^{-7}	411.53	0.0004115	5×10^{-6}	−5.00%	−1.00	−4.00

Table A1. *Cont.*

S_mol_s	D_m2_s	k_s−1	Lambda _calc_ formula	Thresh-old_uM	Texp_s	Thresh-old_ mol_m3	4π*D_r *C_seuil	r_crit _um	r_guess _m	C_calc	Absolute Error (AE) ξ = C_calc − C_threshold	Relative Error (RE)	Log Error
1×10^{-15}	2×10^{-9}	0.1	0.000134	200	10,000	0.2	2.21×10^{-7}	278.11	0.0002781	2×10^{-5}	−20.00%	−1.00	−4.00
1×10^{-15}	1×10^{-10}	30	1.83×10^{-6}	15	60	0.015	5.31×10^{-5}	10.44	1.044×10^{-5}	0.00025	−1.48%	−0.98	−1.78
1×10^{-15}	1×10^{-10}	30	1.83×10^{-6}	50	60	0.05	1.59×10^{-5}	8.60	8.599×10^{-6}	0.00083	−4.92%	−0.98	−1.78
1×10^{-15}	1×10^{-10}	30	1.83×10^{-6}	200	60	0.2	3.98×10^{-6}	6.56	6.562×10^{-6}	0.00333	−19.67%	−0.98	−1.78
1×10^{-15}	1×10^{-10}	30	1.83×10^{-6}	15	3600	0.015	5.31×10^{-5}	17.03	1.703×10^{-5}	4.2×10^{-6}	−1.50%	−1.00	−3.56
1×10^{-15}	1×10^{-10}	30	1.83×10^{-6}	50	3600	0.05	1.59×10^{-5}	15.05	1.505×10^{-5}	1.4×10^{-5}	−5.00%	−1.00	−3.56
1×10^{-15}	1×10^{-10}	30	1.83×10^{-6}	200	3600	0.2	3.98×10^{-6}	12.82	1.282×10^{-5}	5.6×10^{-5}	−19.99%	−1.00	−3.56
1×10^{-15}	1×10^{-10}	30	1.83×10^{-6}	15	10,000	0.015	5.31×10^{-5}	18.72	1.872×10^{-5}	1.5×10^{-6}	−1.50%	−1.00	−4.00
1×10^{-15}	1×10^{-10}	30	1.83×10^{-6}	50	10,000	0.05	1.59×10^{-5}	16.73	1.673×10^{-5}	5×10^{-6}	−5.00%	−1.00	−4.00
1×10^{-15}	1×10^{-10}	30	1.83×10^{-6}	200	10,000	0.2	3.98×10^{-6}	14.46	1.446×10^{-5}	2×10^{-5}	−20.00%	−1.00	−4.00
1×10^{-15}	1×10^{-10}	3	5.77×10^{-6}	15	60	0.015	5.31×10^{-5}	27.44	2.744×10^{-5}	0.00025	−1.48%	−0.98	−1.78
1×10^{-15}	1×10^{-10}	3	5.77×10^{-6}	50	60	0.05	1.59×10^{-5}	21.82	2.182×10^{-5}	0.00083	−4.92%	−0.98	−1.78
1×10^{-15}	1×10^{-10}	3	5.77×10^{-6}	200	60	0.2	3.98×10^{-6}	15.71	1.571×10^{-5}	0.00333	−19.67%	−0.98	−1.78
1×10^{-15}	1×10^{-10}	3	5.77×10^{-6}	15	3600	0.015	5.31×10^{-5}	47.87	4.787×10^{-5}	4.2×10^{-6}	−1.50%	−1.00	−3.56
1×10^{-15}	1×10^{-10}	3	5.77×10^{-6}	50	3600	0.05	1.59×10^{-5}	41.71	4.171×10^{-5}	1.4×10^{-5}	−5.00%	−1.00	−3.56
1×10^{-15}	1×10^{-10}	3	5.77×10^{-6}	200	3600	0.2	3.98×10^{-6}	34.76	3.476×10^{-5}	5.6×10^{-5}	−19.99%	−1.00	−3.56
1×10^{-15}	1×10^{-10}	3	5.77×10^{-6}	15	10,000	0.015	5.31×10^{-5}	53.16	5.316×10^{-5}	1.5×10^{-6}	−1.50%	−1.00	−4.00
1×10^{-15}	1×10^{-10}	3	5.77×10^{-6}	50	10,000	0.05	1.59×10^{-5}	46.93	4.693×10^{-5}	5×10^{-6}	−5.00%	−1.00	−4.00
1×10^{-15}	1×10^{-10}	3	5.77×10^{-6}	200	10,000	0.2	3.98×10^{-6}	39.87	3.987×10^{-5}	2×10^{-5}	−20.00%	−1.00	−4.00
1×10^{-15}	1×10^{-10}	0.1	3.16×10^{-5}	15	60	0.015	5.31×10^{-5}	107.22	0.0001072	0.00025	−1.48%	−0.98	−1.78
1×10^{-15}	1×10^{-10}	0.1	3.16×10^{-5}	50	60	0.05	1.59×10^{-5}	78.86	7.886×10^{-5}	0.00083	−4.92%	−0.98	−1.78
1×10^{-15}	1×10^{-10}	0.1	3.16×10^{-5}	200	60	0.2	3.98×10^{-6}	49.66	4.966×10^{-5}	0.00333	−19.67%	−0.98	−1.78
1×10^{-15}	1×10^{-10}	0.1	3.16×10^{-5}	15	3600	0.015	5.31×10^{-5}	214.74	0.0002147	4.2×10^{-6}	−1.50%	−1.00	−3.56
1×10^{-15}	1×10^{-10}	0.1	3.16×10^{-5}	50	3600	0.05	1.59×10^{-5}	181.91	0.0001819	1.4×10^{-5}	−5.00%	−1.00	−3.56
1×10^{-15}	1×10^{-10}	0.1	3.16×10^{-5}	200	3600	0.2	3.98×10^{-6}	145.20	0.0001452	5.6×10^{-5}	−19.99%	−1.00	−3.56
1×10^{-15}	1×10^{-10}	0.1	3.16×10^{-5}	15	10,000	0.015	5.31×10^{-5}	243.12	0.0002431	1.5×10^{-6}	−1.50%	−1.00	−4.00
1×10^{-15}	1×10^{-10}	0.1	3.16×10^{-5}	50	10,000	0.05	1.59×10^{-5}	209.72	0.0002097	5×10^{-6}	−5.00%	−1.00	−4.00
1×10^{-15}	1×10^{-10}	0.1	3.16×10^{-5}	200	10,000	0.2	3.98×10^{-6}	172.13	0.0001721	2×10^{-5}	−20.00%	−1.00	−4.00
1×10^{-18}	2×10^{-9}	30	7.75×10^{-6}	15	60	0.015	2.95×10^{-9}	0.17	1.729×10^{-7}	0.00025	−1.48%	−0.98	−1.78

Table A1. *Cont.*

S_mol_s	D_m2_s	k_s−1	Lambda_calc_formula	Threshold_uM	Texp_s	Threshold_mol_m3	4π*D_r*C_seuil	r_crit_um	r_guess_m	C_calc	Absolute Error (AE) ξ = C_calc − C_threshold	Relative Error (RE)	Log Error
1×10^{-18}	2×10^{-9}	30	7.75×10^{-6}	50	60	0.05	8.84×10^{-10}	0.10	0.0000001	0.00044	−4.96%	−0.99	−2.06
1×10^{-18}	2×10^{-9}	30	7.75×10^{-6}	200	60	0.2	2.21×10^{-10}	0.10	0.0000001	0.00044	−19.96%	−1.00	−2.66
1×10^{-18}	2×10^{-9}	30	7.75×10^{-6}	15	3600	0.015	2.95×10^{-9}	5.33	5.331×10^{-6}	4.2×10^{-6}	−1.50%	−1.00	−3.56
1×10^{-18}	2×10^{-9}	30	7.75×10^{-6}	50	3600	0.05	8.84×10^{-10}	2.35	2.35×10^{-6}	1.4×10^{-5}	−5.00%	−1.00	−3.56
1×10^{-18}	2×10^{-9}	30	7.75×10^{-6}	200	3600	0.2	2.21×10^{-10}	0.72	7.247×10^{-7}	5.6×10^{-5}	−19.99%	−1.00	−3.56
1×10^{-18}	2×10^{-9}	30	7.75×10^{-6}	15	10,000	0.015	2.95×10^{-9}	9.10	9.102×10^{-6}	1.5×10^{-6}	−1.50%	−1.00	−4.00
1×10^{-18}	2×10^{-9}	30	7.75×10^{-6}	50	10,000	0.05	8.84×10^{-10}	4.77	4.774×10^{-6}	5×10^{-6}	−5.00%	−1.00	−4.00
1×10^{-18}	2×10^{-9}	30	7.75×10^{-6}	200	10,000	0.2	2.21×10^{-10}	1.76	1.761×10^{-6}	2×10^{-5}	−20.00%	−1.00	−4.00
1×10^{-18}	2×10^{-9}	3	2.45×10^{-5}	15	60	0.015	2.95×10^{-9}	0.18	1.756×10^{-7}	0.00025	−1.48%	−0.98	−1.78
1×10^{-18}	2×10^{-9}	3	2.45×10^{-5}	50	60	0.05	8.84×10^{-10}	0.10	0.0000001	0.00044	−4.96%	−0.99	−2.06
1×10^{-18}	2×10^{-9}	3	2.45×10^{-5}	200	60	0.2	2.21×10^{-10}	0.10	0.0000001	0.00044	−19.96%	−1.00	−2.66
1×10^{-18}	2×10^{-9}	3	2.45×10^{-5}	15	3600	0.015	2.95×10^{-9}	7.74	7.737×10^{-6}	4.2×10^{-6}	−1.50%	−1.00	−3.56
1×10^{-18}	2×10^{-9}	3	2.45×10^{-5}	50	3600	0.05	8.84×10^{-10}	2.84	2.835×10^{-6}	1.4×10^{-5}	−5.00%	−1.00	−3.56
1×10^{-18}	2×10^{-9}	3	2.45×10^{-5}	200	3600	0.2	2.21×10^{-10}	0.77	7.711×10^{-7}	5.6×10^{-5}	−19.99%	−1.00	−3.56
1×10^{-18}	2×10^{-9}	3	2.45×10^{-5}	15	10,000	0.015	2.95×10^{-9}	15.59	1.559×10^{-5}	1.5×10^{-6}	−1.50%	−1.00	−4.00
1×10^{-18}	2×10^{-9}	3	2.45×10^{-5}	50	10,000	0.05	8.84×10^{-10}	6.72	6.72×10^{-6}	5×10^{-6}	−5.00%	−1.00	−4.00
1×10^{-18}	2×10^{-9}	3	2.45×10^{-5}	200	10,000	0.2	2.21×10^{-10}	2.03	2.034×10^{-6}	2×10^{-5}	−20.00%	−1.00	−4.00
1×10^{-18}	2×10^{-9}	0.1	0.000134	15	60	0.015	2.95×10^{-9}	0.18	1.766×10^{-7}	0.00025	−1.48%	−0.98	−1.78
1×10^{-18}	2×10^{-9}	0.1	0.000134	50	60	0.05	8.84×10^{-10}	0.10	0.0000001	0.00044	−4.96%	−0.99	−2.05
1×10^{-18}	2×10^{-9}	0.1	0.000134	200	60	0.2	2.21×10^{-10}	0.10	0.0000001	0.00044	−19.96%	−1.00	−2.66
1×10^{-18}	2×10^{-9}	0.1	0.000134	15	3600	0.015	2.95×10^{-9}	9.86	9.859×10^{-6}	4.2×10^{-6}	−1.50%	−1.00	−3.56
1×10^{-18}	2×10^{-9}	0.1	0.000134	50	3600	0.05	8.84×10^{-10}	3.11	3.11×10^{-6}	1.4×10^{-5}	−5.00%	−1.00	−3.56
1×10^{-18}	2×10^{-9}	0.1	0.000134	200	3600	0.2	2.21×10^{-10}	0.79	7.911×10^{-7}	5.6×10^{-5}	−19.99%	−1.00	−3.56
1×10^{-18}	2×10^{-9}	0.1	0.000134	15	10,000	0.015	2.95×10^{-9}	24.55	2.455×10^{-5}	1.5×10^{-6}	−1.50%	−1.00	−4.00
1×10^{-18}	2×10^{-9}	0.1	0.000134	50	10,000	0.05	8.84×10^{-10}	8.31	8.311×10^{-6}	5×10^{-6}	−5.00%	−1.00	−4.00
1×10^{-18}	2×10^{-9}	0.1	0.000134	200	10,000	0.2	2.21×10^{-10}	2.17	2.175×10^{-6}	2×10^{-5}	−20.00%	−1.00	−4.00
1×10^{-18}	1×10^{-10}	30	1.83×10^{-6}	15	60	0.015	5.31×10^{-8}	1.44	1.444×10^{-6}	0.00025	−1.48%	−0.98	−1.78
1×10^{-18}	1×10^{-10}	30	1.83×10^{-6}	50	60	0.05	1.59×10^{-8}	0.66	6.638×10^{-7}	0.00083	−4.92%	−0.98	−1.78

Table A1. *Cont.*

S_mol_s	D_m2_s	k_s−1	Lambda_calc_formula	Threshold_uM	Texp_s	Threshold_mol_m3	4π*D_r*C_seuil	r_crit_um	r_guess_m	C_calc	Absolute Error (AE) ξ = C_calc − C_threshold	Relative Error (RE)	Log Error
1×10^{-18}	1×10^{-10}	30	1.83×10^{-6}	200	60	0.2	3.98×10^{-9}	0.21	2.125×10^{-7}	0.00333	−19.67%	−0.98	−1.78
1×10^{-18}	1×10^{-10}	30	1.83×10^{-6}	15	3600	0.015	5.31×10^{-8}	6.24	6.245×10^{-6}	4.2×10^{-6}	−1.50%	−1.00	−3.56
1×10^{-18}	1×10^{-10}	30	1.83×10^{-6}	50	3600	0.05	1.59×10^{-8}	4.60	4.603×10^{-6}	1.4×10^{-5}	−5.00%	−1.00	−3.56
1×10^{-18}	1×10^{-10}	30	1.83×10^{-6}	200	3600	0.2	3.98×10^{-9}	2.91	2.91×10^{-6}	5.6×10^{-5}	−19.99%	−1.00	−3.56
1×10^{-18}	1×10^{-10}	30	1.83×10^{-6}	15	10,000	0.015	5.31×10^{-8}	7.72	7.722×10^{-6}	1.5×10^{-6}	−1.50%	−1.00	−4.00
1×10^{-18}	1×10^{-10}	30	1.83×10^{-6}	50	10,000	0.05	1.59×10^{-8}	5.99	5.989×10^{-6}	5×10^{-6}	−5.00%	−1.00	−4.00
1×10^{-18}	1×10^{-10}	30	1.83×10^{-6}	200	10,000	0.2	3.98×10^{-9}	4.13	4.134×10^{-6}	2×10^{-5}	−20.00%	−1.00	−4.00
1×10^{-18}	1×10^{-10}	3	5.77×10^{-6}	15	60	0.015	5.31×10^{-8}	2.18	2.181×10^{-6}	0.00025	−1.48%	−0.98	−1.78
1×10^{-18}	1×10^{-10}	3	5.77×10^{-6}	50	60	0.05	1.59×10^{-8}	0.83	8.274×10^{-7}	0.00083	−4.92%	−0.98	−1.78
1×10^{-18}	1×10^{-10}	3	5.77×10^{-6}	200	60	0.2	3.98×10^{-9}	0.23	2.294×10^{-7}	0.00333	−19.67%	−0.98	−1.78
1×10^{-18}	1×10^{-10}	3	5.77×10^{-6}	15	3600	0.015	5.31×10^{-8}	14.78	1.478×10^{-5}	4.2×10^{-6}	−1.50%	−1.00	−3.56
1×10^{-18}	1×10^{-10}	3	5.77×10^{-6}	50	3600	0.05	1.59×10^{-8}	10.05	1.005×10^{-5}	1.4×10^{-5}	−5.00%	−1.00	−3.56
1×10^{-18}	1×10^{-10}	3	5.77×10^{-6}	200	3600	0.2	3.98×10^{-9}	5.51	5.513×10^{-6}	5.6×10^{-5}	−19.99%	−1.00	−3.56
1×10^{-18}	1×10^{-10}	3	5.77×10^{-6}	15	10,000	0.015	5.31×10^{-8}	19.17	1.917×10^{-5}	1.5×10^{-6}	−1.50%	−1.00	−4.00
1×10^{-18}	1×10^{-10}	3	5.77×10^{-6}	50	10,000	0.05	1.59×10^{-8}	14.02	1.402×10^{-5}	5×10^{-6}	−5.00%	−1.00	−4.00
1×10^{-18}	1×10^{-10}	3	5.77×10^{-6}	200	10,000	0.2	3.98×10^{-9}	8.75	8.746×10^{-6}	2×10^{-5}	−20.00%	−1.00	−4.00
1×10^{-18}	1×10^{-10}	0.1	3.16×10^{-5}	15	60	0.015	5.31×10^{-8}	2.90	2.904×10^{-6}	0.00025	−1.48%	−0.98	−1.78
1×10^{-18}	1×10^{-10}	0.1	3.16×10^{-5}	50	60	0.05	1.59×10^{-8}	0.93	9.273×10^{-7}	0.00083	−4.92%	−0.98	−1.78
1×10^{-18}	1×10^{-10}	0.1	3.16×10^{-5}	200	60	0.2	3.98×10^{-9}	0.24	2.37×10^{-7}	0.00333	−19.67%	−0.98	−1.78
1×10^{-18}	1×10^{-10}	0.1	3.16×10^{-5}	15	3600	0.015	5.31×10^{-8}	45.42	4.542×10^{-5}	4.2×10^{-6}	−1.50%	−1.00	−3.56
1×10^{-18}	1×10^{-10}	0.1	3.16×10^{-5}	50	3600	0.05	1.59×10^{-8}	25.54	2.554×10^{-5}	1.4×10^{-5}	−5.00%	−1.00	−3.56
1×10^{-18}	1×10^{-10}	0.1	3.16×10^{-5}	200	3600	0.2	3.98×10^{-9}	10.33	1.033×10^{-5}	5.6×10^{-5}	−19.99%	−1.00	−3.56
1×10^{-18}	1×10^{-10}	0.1	3.16×10^{-5}	15	10,000	0.015	5.31×10^{-8}	65.94	6.594×10^{-5}	1.5×10^{-6}	−1.50%	−1.00	−4.00
1×10^{-18}	1×10^{-10}	0.1	3.16×10^{-5}	50	10,000	0.05	1.59×10^{-8}	42.07	4.207×10^{-5}	5×10^{-6}	−5.00%	−1.00	−4.00
1×10^{-18}	1×10^{-10}	0.1	3.16×10^{-5}	200	10,000	0.2	3.98×10^{-9}	20.69	2.069×10^{-5}	2×10^{-5}	−20.00%	−1.00	−4.00

Appendix A.2

Table A2. Simulated critical distance and calculated threshold for estimated parameters (k and threshold).

Weight (kg)	χ_rad	ΔH_c (M/kg)	E_0	τ	T_amb	t_exp (min)	D_th (°C·min)	D_th/t_exp -(T_amb−37)	r^2	r
100	0.3	46.35	1390.5	0.9	25	1	100	112.00	0.89	0.94
1000	0.3	46.35	13,905	0.9	25	1	100	112.00	8.89	2.98
10,000	0.3	46.35	139,050	0.9	25	1	100	112.00	88.92	9.43
100	0.3	46.35	1390.5	0.9	25	15	100	18.67	5.34	2.31
1000	0.3	46.35	13,905	0.9	25	15	100	18.67	53.35	7.30
10,000	0.3	46.35	139,050	0.9	25	15	100	18.67	533.50	23.10
100	0.3	46.35	1390.5	0.9	25	60	100	13.67	7.29	2.70
1000	0.3	46.35	13,905	0.9	25	60	100	13.67	72.87	8.54
10,000	0.3	46.35	139,050	0.9	25	60	100	13.67	728.69	26.99
100	0.3	46.35	1390.5	0.9	25	120	100	12.83	7.76	2.79
1000	0.3	46.35	13,905	0.9	25	120	100	12.83	77.60	8.81
10,000	0.3	46.35	139,050	0.9	25	120	100	12.83	776.00	27.86
100	0.3	46.35	1390.5	0.9	25	1	200	212.00	0.47	0.69
1000	0.3	46.35	13,905	0.9	25	1	200	212.00	4.70	2.17
10,000	0.3	46.35	139,050	0.9	25	1	200	212.00	46.98	6.85
100	0.3	46.35	1390.5	0.9	25	15	200	25.33	3.93	1.98
1000	0.3	46.35	13,905	0.9	25	15	200	25.33	39.31	6.27
10,000	0.3	46.35	139,050	0.9	25	15	200	25.33	393.11	19.83
100	0.3	46.35	1390.5	0.9	25	60	200	15.33	6.49	2.55
1000	0.3	46.35	13,905	0.9	25	60	200	15.33	64.95	8.06
10,000	0.3	46.35	139,050	0.9	25	60	200	15.33	649.48	25.48
100	0.3	46.35	1390.5	0.9	25	120	200	13.67	7.29	2.70
1000	0.3	46.35	13,905	0.9	25	120	200	13.67	72.87	8.54
10,000	0.3	46.35	139,050	0.9	25	120	200	13.67	728.69	26.99
100	0.3	46.35	1390.5	0.9	25	1	500	512.00	0.19	0.44
1000	0.3	46.35	13,905	0.9	25	1	500	512.00	1.95	1.39
10,000	0.3	46.35	139,050	0.9	25	1	500	512.00	19.45	4.41
100	0.3	46.35	1390.5	0.9	25	15	500	45.33	2.20	1.48
1000	0.3	46.35	13,905	0.9	25	15	500	45.33	21.97	4.69
10,000	0.3	46.35	139,050	0.9	25	15	500	45.33	219.68	14.82
100	0.3	46.35	1390.5	0.9	25	60	500	20.33	4.90	2.21
1000	0.3	46.35	13,905	0.9	25	60	500	20.33	48.98	7.00
10,000	0.3	46.35	139,050	0.9	25	60	500	20.33	489.77	22.13
100	0.3	46.35	1390.5	0.9	25	120	500	16.17	6.16	2.48
1000	0.3	46.35	13,905	0.9	25	120	500	16.17	61.60	7.85
10,000	0.3	46.35	139,050	0.9	25	120	500	16.17	616.00	24.82

References

1. Procopé, B.J. Effect of Repeated Increase of Body Temperature on Human Sperm Cells. *Int. J. Fertil.* **1965**, *10*, 333–339. [PubMed]
2. Davis, J.R.; Horowitz, A.M. Effects of Hyperthermia and Hypothermia on Spontaneous Contractions of the Adult Rabbit Testicular Capsule. *Int. J. Biometeorol.* **1978**, *22*, 303–311. [CrossRef] [PubMed]
3. Glover, T.D.; Young, D.H. Temperature and the Production of Spermatozoa. *Fertil. Steril.* **1963**, *14*, 441–450. [CrossRef] [PubMed]
4. Dada, R.; Gupta, N.P.; Kucheria, K. Spermatogenic Arrest in Men with Testicular Hyperthermia. *Teratog. Carcinog. Mutagen.* **2003**, *23*, 235–243. [CrossRef] [PubMed]
5. Levine, R.J. Male Fertility in Hot Environment. *JAMA* **1984**, *252*, 3250. [CrossRef]
6. Radakovic, S.S.; Maric, J.; Surbatovic, M.; Radjen, S.; Stefanova, E.; Stankovic, N.; Filipovic, N. Effects of Acclimation on Cognitive Performance in Soldiers during Exertional Heat Stress. *Mil. Med.* **2007**, *172*, 133–136. [CrossRef] [PubMed]
7. Jung, A.; Schuppe, H.-C. Influence of Genital Heat Stress on Semen Quality in Humans. *Andrologia* **2007**, *39*, 203–215. [CrossRef] [PubMed]
8. Mieusset, R.; Bujan, L.; Mansat, A.; Pontonnier, F.; Grandjean, H. Effects of Artificial Cryptorchidism on Sperm Morphology*. *Fertil. Steril.* **1987**, *47*, 150–155. [CrossRef]
9. Henderson, J.; Baker, H.W.; Hanna, P.J. Occupation-Related Male Infertility: A Review. *Clin. Reprod. Fertil.* **1986**, *4*, 87–106. [CrossRef]
10. Dorman, S.C.; Lessel, C. *Stress Thermique Guide de Sensibilisation*; Gagnon, D., Kanya-Forstner, M., Eds.; Centre or Research in Occupational Safety and Health: Sudbury, ON, Canada, 2024.
11. du Plessis, S.S.; McAllister, D.A.; Luu, A.; Savia, J.; Agarwal, A.; Lampiao, F. Effects of H_2O_2 Exposure on Human Sperm Motility Parameters, Reactive Oxygen Species Levels and Nitric Oxide Levels. *Andrologia* **2010**, *42*, 206–210. [CrossRef] [PubMed]
12. Aitken, R.J.; Drevet, J.R. The Importance of Oxidative Stress in Determining the Functionality of Mammalian Spermatozoa: A Two-Edged Sword. *Antioxidants* **2020**, *9*, 111. [CrossRef] [PubMed]
13. Agarwal, A.; Roychoudhury, S.; Bjugstad, K.B.; Cho, C.-L. Oxidation-Reduction Potential of Semen: What Is Its Role in the Treatment of Male Infertility? *Ther. Adv. Urol.* **2016**, *8*, 302–318. [CrossRef] [PubMed]
14. Abouelouafa, M.; Ossmani, H.E.; Bakri, Y.; Omari, S.; Mbarki, A. Thermal Radiation Impact on Cellular Viability: Comparative Modeling of Tolerable and Lethal Distances Using Probit Methods. *Perinat. J.* **2026**, *34*, 1113–1123. [CrossRef]
15. Sadeghi, S.; Pertusa, J.; Yaniz, J.L.; Nuñez, J.; Soler, C.; Silvestre, M.A. Effect of Different Oxidative Stress Degrees Generated by Hydrogen Peroxide on Motility and DNA Fragmentation of Zebrafish (Danio Rerio) Spermatozoa. *Reprod. Domest. Anim.* **2018**, *53*, 1498–1505. [CrossRef] [PubMed]
16. De Iuliis, G.N.; Thomson, L.K.; Mitchell, L.A.; Finnie, J.M.; Koppers, A.J.; Hedges, A.; Nixon, B.; Aitken, R.J. DNA Damage in Human Spermatozoa Is Highly Correlated with the Efficiency of Chromatin Remodeling and the Formation of 8-Hydroxy-2′-Deoxyguanosine, a Marker of Oxidative Stress. *Biol. Reprod.* **2009**, *81*, 517–524. [CrossRef] [PubMed]
17. Koppers, A.J.; De Iuliis, G.N.; Finnie, J.M.; McLaughlin, E.A.; Aitken, R.J. Significance of Mitochondrial Reactive Oxygen Species in the Generation of Oxidative Stress in Spermatozoa. *J. Clin. Endocrinol. Metab.* **2008**, *93*, 3199–3207. [CrossRef] [PubMed]
18. Fonseca, A.C.S.; Barreiro, M.; Tomé, A.; Vale-Fernandes, E. Male Reproductive Health—Study of a Sperm Donor Population. *JBRA Assist. Reprod.* **2022**, *26*, 247–254. [CrossRef] [PubMed]
19. Emploi et Développement Social Canada. Le Stress Thermique dans les Lieux de Travail. Available online: https://www.canada.ca/fr/emploi-developpement-social/services/sante-securite/rapports/stress-thermique-lieux-travail.html (accessed on 8 October 2025).
20. Finney, D.J. *Probit Analysis*, 3rd ed.; University Press: Cambridge, UK, 1971.
21. Wu, Y.-Q.; Rao, M.; Hu, S.-F.; Ke, D.-D.; Zhu, C.-H.; Xia, W. Effect of Transient Scrotal Hyperthermia on Human Sperm: An iTRAQ-Based Proteomic Analysis. *Reprod. Biol. Endocrinol.* **2020**, *18*, 83. [CrossRef] [PubMed]
22. Rao, M.; Zhao, X.-L.; Yang, J.; Hu, S.-F.; Lei, H.; Xia, W.; Zhu, C.-H. Effect of Transient Scrotal Hyperthermia on Sperm Parameters, Seminal Plasma Biochemical Markers, and Oxidative Stress in Men. *Asian J. Androl.* **2015**, *17*, 668–675. [CrossRef] [PubMed]
23. Khayyam, O. Chapter 7: Vulnerability Models. In *Process Systems Risk Management*; Elsevier: Amsterdam, The Netherlands, 2005.
24. Poblete, B.R.; Lees, F.P.; Simpson, G.B. The Assessment of Major Hazards: Estimation of Injury and Damage around a Hazard Source Using an Impact Model Based on Inverse Square Law and Probit Relations. *J. Hazard. Mater.* **1984**, *9*, 355–371. [CrossRef]
25. Crank, J. *The Mathematics of Diffusion*, 2nd ed.; Oxford University Press: Oxford, NY, USA, 1979.
26. Chaki, S.P.; Misro, M.M. Assessment of Human Sperm Function after Hydrogen Peroxide Exposure: Development of a Vaginal Contraceptive. *Contraception* **2002**, *66*, 187–192. [CrossRef] [PubMed]
27. Domínguez-Rebolledo, A.E.; Martínez-Pastor, F.; Bisbal, A.F.; Ros-Santaella, J.L.; García-Álvarez, O.; Maroto-Morales, A.; Soler, A.J.; Garde, J.J.; Fernández-Santos, M.R. Response of Thawed Epididymal Red Deer Spermatozoa to Increasing Concentrations of Hydrogen Peroxide, and Importance of Individual Male Variability. *Reprod. Domest. Anim.* **2011**, *46*, 393–403. [CrossRef] [PubMed]
28. Ryu, D.-Y.; Kim, K.-U.; Kwon, W.-S.; Rahman, M.S.; Khatun, A.; Pang, M.-G. Peroxiredoxin Activity Is a Major Landmark of Male Fertility. *Sci. Rep.* **2017**, *7*, 17174. [CrossRef] [PubMed]

29. Fernandez, M.C.; O'Flaherty, C. Peroxiredoxin 6 Is the Primary Antioxidant Enzyme for the Maintenance of Viability and DNA Integrity in Human Spermatozoa. *Hum. Reprod.* **2018**, *33*, 1394–1407. [CrossRef] [PubMed]
30. Bienert, G.P.; Møller, A.L.B.; Kristiansen, K.A.; Schulz, A.; Møller, I.M.; Schjoerring, J.K.; Jahn, T.P. Specific Aquaporins Facilitate the Diffusion of Hydrogen Peroxide across Membranes*. *J. Biol. Chem.* **2007**, *282*, 1183–1192. [CrossRef] [PubMed]
31. Kemal Duru, N.; Morshedi, M.; Oehninger, S. Effects of Hydrogen Peroxide on DNA and Plasma Membrane Integrity of Human Spermatozoa. *Fertil. Steril.* **2000**, *74*, 1200–1207. [CrossRef] [PubMed]
32. Pujianto, D.A.; Oktarina, M.; Sharma Sharaswati, I.A.; Yulhasri. Hydrogen Peroxide Has Adverse Effects on Human Sperm Quality Parameters, Induces Apoptosis, and Reduces Survival. *J. Hum. Reprod. Sci.* **2021**, *14*, 121–128. [CrossRef] [PubMed]
33. O'Flaherty, C.; Rico de Souza, A. Hydrogen Peroxide Modifies Human Sperm Peroxiredoxins in a Dose-Dependent Manner. *Biol. Reprod.* **2011**, *84*, 238–247. [CrossRef] [PubMed]
34. Thakor, H.P.; Verma, A.; Elango, K.; Gv, V.; Manimaran, A.; Jeyakumar, S.; Kumaresan, A. Effect of Different Concentrations of Hydrogen Peroxide on Indigenous Bull Sperm Motility. *Int. J. Vet. Sci. Anim. Husb.* **2024**, *9*, 881–884. [CrossRef]
35. Ledo, A.; Fernandes, E.; Salvador, A.; Laranjinha, J.; Barbosa, R.M. In Vivo Hydrogen Peroxide Diffusivity in Brain Tissue Supports Volume Signaling Activity. *Redox Biol.* **2022**, *50*, 102250. [CrossRef] [PubMed]
36. Bienert, G.P.; Chaumont, F. Aquaporin-Facilitated Transmembrane Diffusion of Hydrogen Peroxide. *Biochim. Biophys. Acta* **2014**, *1840*, 1596–1604. [CrossRef] [PubMed]
37. Gerich, F.J.; Funke, F.; Hildebrandt, B.; Faßhauer, M.; Müller, M. H2O2-Mediated Modulation of Cytosolic Signaling and Organelle Function in Rat Hippocampus. *Pflug. Arch.* **2009**, *458*, 937–952. [CrossRef] [PubMed]
38. O'Flaherty, C. Peroxiredoxins: Hidden Players in the Antioxidant Defence of Human Spermatozoa. *Basic Clin. Androl.* **2014**, *24*, 4. [CrossRef] [PubMed]
39. Mbarki, A.; Ettahir, A.; Guelzim, A. Determination of The Thermal Lethality Distances Generated by The Radiative Flux Emitted by The Di-Tert-Butyl Peroxide (DTBP, C8H18O2) Fireball: Use of Characteristic Curves. *IOP Conf. Ser. Earth Environ. Sci.* **2022**, *1050*, 012018. [CrossRef]
40. Mbarki, A.; Ettahir, A.; Guelzim, A. Delineation of the Thermal Effect Zones Generated by the Radiation Emitted by the Fireball of an LPG BLEVE, Using the Characteristic Curves of Lee's Point Source Model. *Int. Rev. Mech. Eng. (IREME)* **2022**, *16*, 222–229. [CrossRef]
41. Guelzim, A.; Ettahir, A.; Mbarki, A. Lee's Model and Determination of the Thermal Effect Zones of an LNG BLEVE Fireball. In *Advances in Clean Energy Systems and Technologies*; Chen, L., Ed.; Springer: Cham, Switzerland, 2024; pp. 305–313.
42. Kurazumi, Y.; Rezgals, L. Convective Heat Transfer Coefficients of the Human Body under Forced Convection from Ceiling. *J. Ergon.* **2014**, *4*, 1000126. [CrossRef]
43. de Dear, R.J.; Arens, E.; Hui, Z.; Oguro, M. Convective and Radiative Heat Transfer Coefficients for Individual Human Body Segments. *Int. J. Biometeorol.* **1997**, *40*, 141–156. [CrossRef] [PubMed]
44. Sheynkin, Y.; Jung, M.; Yoo, P.; Schulsinger, D.; Komaroff, E. Increase in Scrotal Temperature in Laptop Computer Users. *Hum. Reprod.* **2005**, *20*, 452–455. [CrossRef] [PubMed]
45. Sales, K.; Vasudeva, R.; Dickinson, M.E.; Godwin, J.L.; Lumley, A.J.; Michalczyk, Ł.; Hebberecht, L.; Thomas, P.; Franco, A.; Gage, M.J.G. Experimental Heatwaves Compromise Sperm Function and Cause Transgenerational Damage in a Model Insect. *Nat. Commun.* **2018**, *9*, 4771. [CrossRef] [PubMed]
46. Ziaeipour, S.; Piryaei, A.; Aliaghaei, A.; Nazarian, H.; Naserzadeh, P.; Ebrahimi, V.; Abdi, S.; Shahi, F.; Ahmadi, H.; Fadaei Fathabadi, F.; et al. Chronic Scrotal Hyperthermia Induces Azoospermia and Severe Damage to Testicular Tissue in Mice. *Acta Histochem.* **2021**, *123*, 151712. [CrossRef] [PubMed]
47. NICNAS. *Hydrogen Peroxide (H_2O_2): Human Health Tier II Assessment*; IMAP; NICNAS: Sydney, NSW, Australia, 2014; p. 17. Available online: https://www.industrialchemicals.gov.au/ (accessed on 8 October 2025).
48. Wang, X.; Liu, Q.; Zhuang, Z.; Cheng, J.; Zhang, W.; Jiang, Q.; Guo, Y.; Li, R.; Lu, X.; Cui, L.; et al. Decoding the Pathogenesis of Spermatogenic Failure in Cryptorchidism through Single-Cell Transcriptomic Profiling. *Cell Rep. Med.* **2024**, *5*, 101709. [CrossRef] [PubMed]
49. Althubaiti, A.; Donev, A. Non-Gaussian Berkson Errors in Bioassay. *Stat. Methods Med. Res.* **2016**, *25*, 430–445. [CrossRef] [PubMed]
50. Cramer, J. The Origins and Development of the Logit Model. In *Logit Models from Economics and Other Fields*; Cambridge University Press: Cambridge, UK, 2003. [CrossRef]
51. Aitken, R.J. Reactive Oxygen Species as Mediators of Sperm Capacitation and Pathological Damage. *Mol. Reprod. Dev.* **2017**, *84*, 1039–1052. [CrossRef] [PubMed]
52. Rylander, M.N.; Feng, Y.; Bass, J.; Diller, K.R. Thermally Induced Injury and Heat-Shock Protein Expression in Cells and Tissues. *Ann. N. Y. Acad. Sci.* **2006**, *1066*, 222–242. [CrossRef] [PubMed]
53. Pearce, J.A. Comparative Analysis of Mathematical Models of Cell Death and Thermal Damage Processes. *Int. J. Hyperth.* **2013**, *29*, 262–280. [CrossRef] [PubMed]

54. Abouelouafa, M.; Houate, B.E.; Hakem, A.; Mbaye, M.M.; Kabbour, M.; Mbarki, A.; El Ossmani, H.; Bakri, Y. Hormonal Profiles and Y Chromosome AZF Microdeletions in Moroccan Azoospermic Men: A Molecular and Endocrine Study. *Reprod. Med.* **2026**, *7*, 29. [CrossRef]
55. Zhou, L.; Aon, M.A.; Almas, T.; Cortassa, S.; Winslow, R.L.; O'Rourke, B. A Reaction-Diffusion Model of ROS-Induced ROS Release in a Mitochondrial Network. *PLoS Comput. Biol.* **2010**, *6*, e1000657. [CrossRef] [PubMed]

Disclaimer/Publisher's Note: The statements, opinions and data contained in all publications are solely those of the individual author(s) and contributor(s) and not of MDPI and/or the editor(s). MDPI and/or the editor(s) disclaim responsibility for any injury to people or property resulting from any ideas, methods, instructions or products referred to in the content.